UNIVERSITA' POLITECNICA DELLE MARCHE

FACOLTA' DI **INGEGNERIA**

Corso di Laurea magistrale in

BIOMEDICAL ENGENEERING

Tesi di laurea:

fMRI CHARACTERIZATION OF INTRINSIC BRAIN NETWORKS RELEVANT FOR MOTOR CONTROL WITH AND WITHOUT VISUAL FEEDBACK BY FRACTAL DIMENSION

Supervisor:
Prof. **Camillo Porcaro**

Candidate:
Camilla Sala

A.A. **2021 / 2022**

SUMMARY

SUMMARY

Functional magnetic resonance imaging (fMRI) is a class of imaging modalities used to characterize regional, time-varying changes in brain metabolism (Glover, n.d.). These metabolic changes may be the result of task-induced changes in cognitive status or of unregulated processes in the resting brain. Since its introduction in 1990, fMRI has been used in numerous studies in cognitive neuroscience, clinical psychiatry/psychology, and preoperative planning. The popularity of fMRI stems from its wide availability in both clinical and research environments (ranging from 1.5 to 7 Tesla), non-invasiveness (no injection of radioisotopes or other drugs is necessary), and optimal spatial resolution (order of millimeters). fMRI is increasingly used as a biomarker of disease, for treatment monitoring or to study pharmacological efficacy (Glover, n.d.). In recent years functional connectivity study using fMRI (fcMRI) has drawn the increasing attention of neuroscientists and computer scientists, since it opens a new window to explore functional networks of the human brain with relatively high resolution (Li et al. 2008).

Functional connectivity is defined as the "temporal correlations between spatially remote neurophysiological events" (Li et al. 2008) and examines regional interactions in the brain at a macro level, using datasets from electroencephalographic (EEG), magnetoencephalographic (MEG), local field potentials (LFP), positron emission tomography (PET) or fMRI. After extensive study for more than a decade, scientists have come up with several methods for functional connectivity detection using fMRI. Generally, these methods can be classified into two categories: **model-driven and data-driven methods**. For the model-driven methods, strong prior neuroscience knowledge or experience is needed to select some region of interest (ROI) called ''seeds'' and determine whether other regions are connected to these. Data-driven methods are developed to overcome some of these limitations of the model-driven one, indeed these methods are independent of prior information or assumed models (Horovitz et al. 2019). For the data-driven methods, one of the most widespread approach is the Independent component analysis (ICA), which expresses the original neuroimaging dataset as a statistically independent component (Bordier, Dojat, and de Micheaux 2011). Functional connectivity is mandatory especially when activations are spread around the brain, mainly during cognitive processes.

A key to human interaction with the environment is the planning and execution of motor actions to coordinate the body's movements, which is essential for daily actions on objects. The success of such actions depends on the coordination of several complex factors such as visual cues, tactile and skin feedback, control of grip, speed, direction and duration of the force applied on the surface of the object.

Through neuroimaging studies, with the use of fMRI, the organization of brain activity during execution and the coordination of precision and strength has been extensively investigated to clarify the space-time dynamics of these processes and to identify the neural origins of the cognitive components involved in motor control, but also to be the basis of more complex motor studies. The organization of human motor control and the knowledge of its characteristics are also fundamental for the implementation of the Brain-Computer Interface (BCI). (Ortiz-Rosario and Adeli 2013)

It is widely recognized that continuous sensory feedback plays a crucial role in accurate motor control in everyday life. Feedback information is used to adapt force output and to correct errors. While the primary motor cortex contralateral to the movement (cM1) plays a dominant role in this control, converging evidence supports the idea that that ipsilateral primary motor cortex (iM1) also directly contributes to hand and finger movements. Similarly, when visual feedback is available, the primary visual cortex (V1) and its interactions with the motor network also become important for accurate motor performance (Verstynen et al. 2005a). To clarify this issue, we performed and studied measurements obtained during isometric compression of a compliant rubber bulb, at 10% maximum voluntary contraction, both with (visuomotor task) and without visual feedback (motor task).

However, all studies to date use the mass-univariate voxel-based approach, which focuses on segregating and localizing processes, failing to account for the integration across processes within larger networks (Mayhew et al. 2017). The mass univariate voxel-based analysis also relies on subtraction methods between conditions, emphasizing more significant differences than similarities between processes. Functional connectivity analysis is an alternative multivariate method to assess the functional architecture of the central nervous system that integrates brain signals across multiple regions. Among others, this approach uses correlations between distant regions as the dependent variable.

ICA is often used to identify clusters of regions that show high correlations of signal change within a given time window. These clusters are assumed to reflect intrinsic connectivity networks (Porcaro et al. 2020a; Mansi et al. 2022). Consistent intrinsic networks have been repeatedly identified using ICA [21]. These include networks that connect homologous regions processing visual, auditory, and sensory-motor output. These are the default mode network (anterior and posterior midline and inferior parietal); the lateralized dorsal frontal-parietal network, putatively involved in attention; the saliency network which comprises the insula and the anterior cingulum; the frontal network involving prefrontal, frontotemporal, and cingulate cortex, thought to reflect executive control; the left-lateralized ventral, frontal, and parietal network, involved in language processing and the precuneus, basal ganglia, and a cerebellum network. Importantly, similar networks are detected when participants

are engaged in a task (goal-driven behavior) or are free to wander (rest). In addition, differences between rest and specific task conditions are modeled as a reconfiguration of connections within and between networks. It has been argued that the task-based spatial ICA data-driven approach is advantageous over conventional mass-univariate analysis of signal amplitude change. This is because it does not rely on assumptions regarding the time course, the temporal characteristics, and the shape of the hemodynamic response function.

In this thesis, we analyzed fMRI data recorded from sixteen healthy volunteers (Mayhew et al. 2017) using a multivariate data-driven approach focusing on intrinsic connectivity between voxels through group ICA of fMRI Toolbox (GIFT), asking the following main questions:

1. which are the networks involved during a motor task (i.e. without a visual feedback) and a visuomotor task (i.e. with visual feedback)?
2. Is there any hemodynamic signal complexity difference between the visuomotor and the motor task?

Visual network (VN), Frontal Eye Field (FEF), Default Mode Network (DMN), Attention Network (AttN - Salience Network (SN) and Control Executive Network (CEN), Cerebellum (Cb), Basal Ganglia (BG) and Sensorimotor Network (SMN) are the main networks involved during the tasks, with the VN and the FEF mainly involved in the visuomotor task. Interestingly, during the visuomotor task, the involvement of the FEF and the ipsilateral primary motor area (iM1) seems to be essential for the fine motor control of the movement in keeping the force shown by the visual feedback. Moreover, the characterization of the neuronal dynamics of the blood oxygenation level-dependent (BOLD) activity (i.e. the fMRI signal) of the intrinsic networks involved during both tasks (motor and visuomotor task) showed a higher complexity (estimated by Higuchi's Fractal Dimension) of the BOLD activity on the following intrinsic networks (VN, FEF, SMN (in particular the iM1), ExCN, CB) for visuomotor task respect to the pure motor task.

1. NUCLEAR MAGNETIC RESONANCE

1.1 Principles of Nuclear Magnetic Resonance (NMR)

Nuclear magnetic resonance (NMR) is a non-invasive investigation technique that exploits radiation-matter interaction in the radio waves frequency band (Dais, 2012). The principle of this technique is that many nuclei have spin and all nuclei are electrically charged. When an external magnetic field is applied, energy transfer between fundamental energy to higher energy levels (usually a single energy gap) is possible. Energy transfer occurs at wavelengths that correspond to radio frequencies, the same frequency that energy is emitted when the spin returns to its fundamental energy level. The signal corresponding to this transmission is measured and processed in a number of ways to obtain the NMR spectrum of the nucleus in question. It works on nuclear paramagnetic materials, microscopically made of magnetic dipoles spontaneously randomly distributed. It is essential in magnetic resonance that nuclear magnetic moments in the sample align to an external magnetic field in order to obtain a measurable macroscopic. When resonant radiation (whose energy corresponds to the difference between energy levels in a physical system) is sent to that system, the absorbed and emitted radiation provides information about the system itself. The NMR signal is derived from the nuclear spins obtained from the system response after excitation. Degenerate nuclear spin levels, call Zeeman effect, can be split by applying an external static magnetic field, and then using resonant high-frequency pulses to bring the spins to higher energy levels. Therefore, NMR can study matter through the macroscopic magnetization generated by the nuclear magnetic moment aligned with the external magnetic field. Observing subsamples of nuclear paramagnetic species requires an optimized frequency range. The radio frequencies used range from 20MHz to 1GHz, generated digitally and then transmitted from the coil. These radiations are coherent in nature and are characterized by very low energy, allowing high photon fluxes at a given energy, while using wavelengths from millimeters to tenths of a centimeter in water. The importance of radio frequency is that spontaneous emission can be forgotten and stable inversions in the population can be achieved, thereby obtaining information about molecular dynamics from NMR signal quenching. (Louro 2013)

1.2 Physical principles of Magnetic Resonance Imaging (MRI)

MRI is a technique that allows obtaining images of living tissues noninvasively and without using ionizing radiation, by measuring the magnetic spin properties of certain atomic nuclei, mainly hydrogen, due to its important presence in the human, in form of water molecules (Hendee and Morgan 1984). When a nucleus contains either unpaired protons, neutrons, or both, it has angular momentum. This property provides the basis for magnetic resonance imaging (MRI). Because of its

abundance in the human body, hydrogen is used for clinical MRI. Within the MR magnet, the atoms are aligned with the magnetic field (Hendee and Morgan 1984).

MRI enabled to generate anatomical images of human body sections, by recording the minuscule radio signal released by atomic nuclei excited with temporary varying magnetic fields. Protons and neutrons, as we said before, are characterized by an intrinsic angular momentum, or spin, to which is associated a nuclear magnetic moment, processing in correspondence of a given static magnetic field $\vec{B}o$ at the so-called Larmor frequency w_L:

$$w_L = \gamma * \overrightarrow{Bo} \tag{1.1}$$

in which γ represents gyromagnetic ratio, which is equal to 42.57 MHz/T for a hydrogen nucleus. In absence of a strong magnetic field, nuclear magnetic moments are randomly oriented and the overall sum of their magnetic contribution is equal to zero. The presence of the static high-intensity magnetic field, gradually, induces the alignment of the nuclear magnetic moments with or against the main direction of the magnetic field, as shown in Figure 1. If the nuclear magnetic moments display a preferential orientation, while keeping cancelling each other contribution, the net magnetization vector $\vec{M}$ is non-zero ("Physical Principles of Magnetic Resonance Imaging - PubMed" n.d.).

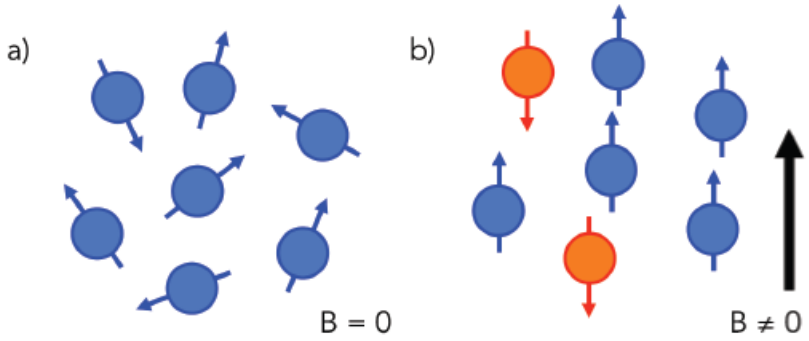

Figure 1. Behavior of nuclear magnetic moments a) in absence and b) in presence of a static magnetic field B. In a), nuclei are randomly oriented and their magnetic contribution is equal to zero, since there is not a preferential direction of alignment. In b), the presence of a magnetic field induces the alignment of nuclear magnetic moments in the direction of the magnetic field, in a parallel or antiparallel fashion.

Though, when a supplementary magnetic field $\vec{B}_1$ is applied (Figure 2), this equilibrium is disrupted and the magnetization vector $\vec{M}$ is tilted proportionally to the exposure duration of the temporary magnetic field. This field is applied in form of electromagnetic wave, and modifies the characteristic Larmor frequency wL associated with the given proton:

$$w_L = \gamma * (\overrightarrow{B_o} + \overrightarrow{B_1}) \tag{1.2}$$

$\vec{M}$ rotates around the main magnetic field vector, through a movement called precession. When an oscillatory magnetic field $\vec{B}_1$ transverse to $\vec{B}_O$ is applied at a frequency similar to Larmor frequency,

it is in resonance with the processing nuclei, which means that the net magnetization $\vec{M}$ changes its equilibrium orientation of a certain angle, flip angle (Seeger 1989).

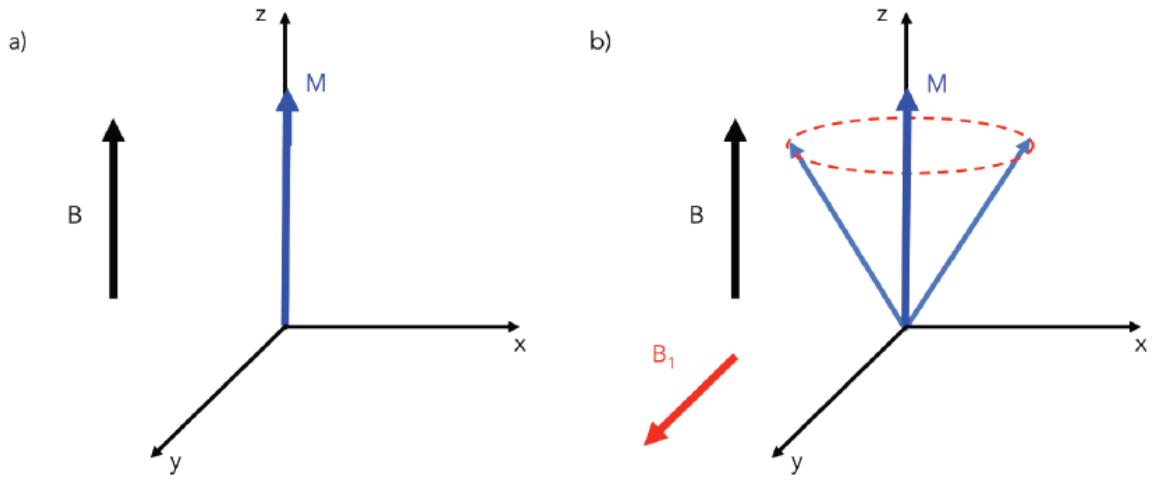

Figure 2. In presence of a static magnetic field B, the magnetization vector M is aligned with B and it has maximum magnitude (a). When a supplementary magnetic field B1 is applied M is tilted of a certain angle proportional to the duration and entity of B1 (b). Both in a) and b), M keeps rotating around its own axis with a movement called precession.

Following this excitation, $M^{\rightarrow}$, by continuing the rotation around the z-axis at the Larmor frequency, presents a longitudinal component MZ and a transversal component Mxy perpendicular to each other. This precession can be detected by a receiver coil, by means of electromagnetic induction, expressed by Faraday's law:

$$\varepsilon_l = -\frac{d\emptyset_s}{dt}(t) = -\frac{d}{dt}\int_S \vec{B}(\vec{r},t) * \vec{N}(\vec{r},t)dS \qquad (1.3)$$

In which ε_l is the induced electromotive force,$\emptyset_S$ represents the magnetic flux through the surface S enclosed by the coil, and $\vec{N}$ he unitary normal vector to the surface S at the position $\vec{n}$ and the instant time $\vec{t}$. When the exciting oscillatory magnetic field is removed, the $\vec{M}$ tends to return to its original state of equilibrium, by dissipating the energy received during the excitation step. Thus, the magnitude of M_Z and M_{xy} does not remain constant in time. In particular, M_Z increases, while M_{xy} becomes again null. This process is called **spin relaxation** and, depending on the way the excited nuclei dissipate their energy, it is possible to differentiate three mechanism (Seeger 1989):

1) T_1 relaxation time constant explicates a process called spin-lattice relaxation, in which excited nuclei dissipate their energy in interactions with surrounding molecules mediated by randomly fluctuating magnetic fields. The T_1 relaxation mechanisms drive the regeneration of the $\vec{M}$ along the z-axis, as described by the following expression:

$$M_Z(t) = M_0 - \left(M_0 - M_Z(0)\right) * e^{-t/T_1} \quad (1.4)$$

In which MZ reaches the maximum value MO corresponding to the $T1$.

2) T_2 relaxation time constant explicates a process called spin-spin relaxation, in which excited nuclei experience small variations in their Larmor frequency, due to low-frequency, microscopic random fluctuations of the local magnetic field. These small individual variations in the Larmor frequency lead to a general loss of phase coherence for the individual magnetic moments, resulting in a decrease of the magnitude of the transverse magnetization M_{xy} , as described by the following expression:

$$M_{xy}(T) = M_{xy}(0) * e^{-t/T_2} \quad (1.5)$$

3) T_2^* mechanisms are associated with differences in Larmor frequency across a sample of nuclei due to "external", macroscopic magnetic field inhomogeneities. These inhomogeneities can be caused by distortions occurring in the static magnetic field, or by differences in magnetic susceptibility between structures in the sample, such as air/tissue interfaces. Due to these differences, their contributions are cancelled by each other, and fast decay of the signal occurs. T_2^*which depends on the field inhomogeneities, can be considerably shorter than T_2 (LL., 1989):

$$\frac{1}{T_2^*} = \frac{1}{T_2} + \frac{1}{T_2'} \quad (1.6)$$

In order to produce an image, the alignment between the static magnetic field B and the magnetization vector is perturbed. Magnetic resonance imaging exploits these physical properties to differentiate tissues, which are characterized by peculiar composition and density. In fact, temporary and spatially varying magnetic fields are used to encode magnetic spins with space-dependent properties, and thereby obtain information regarding their distribution in living tissues. More specifically, magnetic field gradients are applied in the scanner in which the static strong magnetic field is already present. When the supplementary gradient is switched on the magnetic field linearly increases in the selected direction, resulting in variation in Larmor frequency based on the position. Thus, it is possible to focus on the specific sample of interest that presents the defined Larmor frequency (Seeger 1989). Image generation is achieved by combining three types of spatial encoding, i.e. slice selection, phase encoding and frequency encoding, one for each spatial dimension. Accordingly, three different gradient fields along three orthogonal directions are superimposed to the static magnetic field. The slice selection consists in the excitation of certain range of frequencies, centered in W, to which

corresponds a certain slice thickness in the acquired volume. The process is repeated for different values of frequencies, thus for electing different slides, until the full volume of interest is acquired. After the excitation of a slice, based on the echo time, the RF coils detect the signal, associated with the relaxation. The magnetization vector can be described as a complex number, in which magnitude relates to the actual relaxation and the phase to the precession movement. Following the selection of the slice of interest, phase and frequency encoding enable the spatial discrimination on a plane. The phase encoding consists in the application of a gradient G that will introduce a spatially dependent shift. Thus, it is possible to identify differences in position based on the different phases of the detected signal. The frequency encoding is then applied to differentiate the precession frequencies along the x direction. The third gradient is typically applied simultaneously with the actual image acquisition, i.e. Readout. Each tissue is characterized by specific relaxation time, thus by selecting a certain acquisition sequence is possible to enhance or suppress the effect of magnetization given from a certain brain region. By manipulating the acquisition parameters, repetition time (TR), and echo time (TE) the magnetization vector, and, subsequently, the acquired signal, displays differences associated with the time constants T_1 and T_2 , such as contrast or brightness, and enable the discrimination of tissues (Foster et al., 1984), as shown in Figure 3.

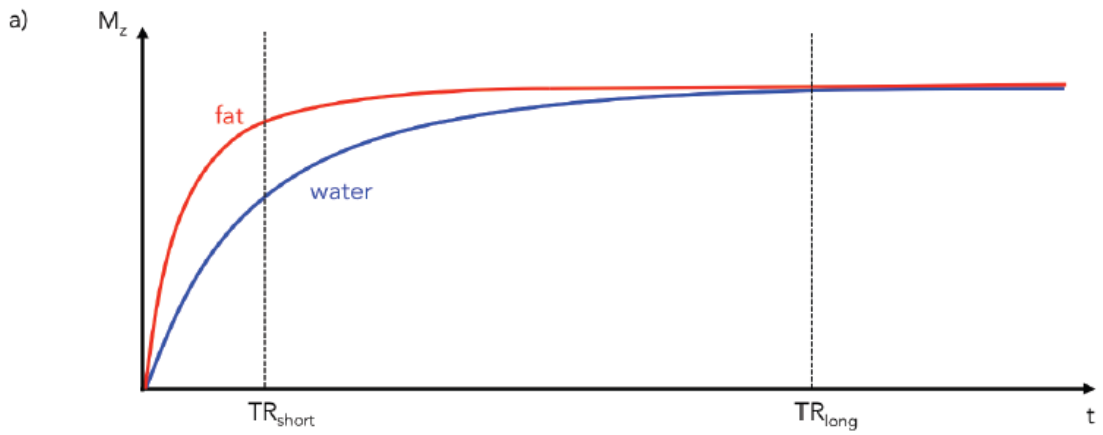

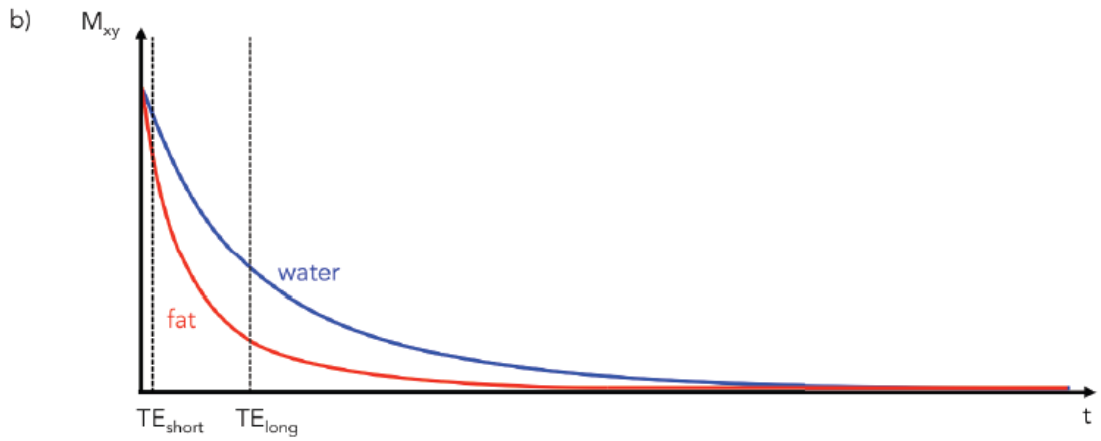

Figure 3. Discrimination of brain tissues based on the contrast associated with specific relaxation times. In a) T1-weighted recovery of different structures is shown. A short TR time provides a larger contrast between two tissues with different composition. A long TR does not allow discriminating the two structures. In b) T2-weighted decay of different structures is shown. A short TE time does not allow discriminating the two structures. A long TR provides a larger contrast between two tissues with different composition.

TR represents the time between two consecutive pulses, and it should be long enough to allow the magnetization vector to restore its equilibrium state. TE is referred to as the time between the initial excitation pulse and the detection of the MR signal.

1.3MRI Scanner

Magnetic resonance imaging (MRI) is a type of scan that uses strong magnetic fields and radio waves to produce detailed images of the inside of the body. An MRI scanner is a large tube that contains powerful magnets. The MR scanner consists of several components, including a cylindrical superconductive magnet that generates the static magnetic field, and radiofrequency (RF) coils which are used to apply the temporary supplementary magnetic gradients and, eventually, to detect the released signal following the relaxation.

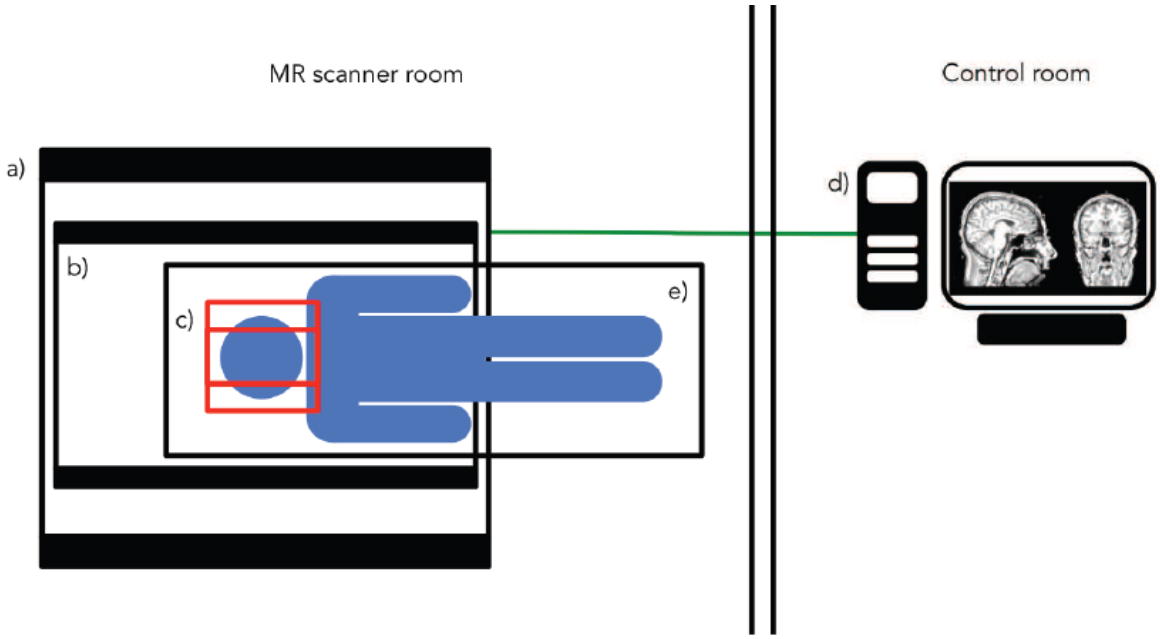

Figure 4 Schematic of an MRI acquisition system, including a) superconductive magnet, which generates the static magnetic field, b) RF coils, which generates the temporally-varying gradients and detect the released signals from the brain, c) head-coil, which constrains the volume of interest to be acquired, d) recording computer on which MR data can be visualized, following the reconstruction of the image, and e) bed on which the subject lies during the investigation in the MR scanner. The MR scanner is located in a shielded room. This is required for safety reasons, for avoiding dangerous situations related to the presence of a free strong magnetic field, and for data quality, for avoiding unwanted distortions in the MR data due to electromagnetic disturbances. Accordingly, only MR compatible electronic device and metal-free objects can be introduced in the MR scanner room. The recording computer is located in the control room, which is typically next to the MR scanner room.

An MRI scan can be used to examine almost any part of the body, including the:

- brain and spinal cord
- bones and joints
- breasts
- heart and blood vessels
- internal organs, such as the liver, womb or prostate gland

The results of an MRI scan can be used to help diagnose conditions, plan treatments and assess how effective previous treatment has been. To preserve its superconductive state, the magnet is kept at very low temperature, just a few Kelvin, by means of a helium pump cooling system, also called cryogenic pump, in addition to several thermally insulating layers. The MR scanner is controlled from a computer located in an external room. In particular, this computer is used to program the specific sequence associated with the acquisition protocol and allows the visualization of the acquired volumes. The triggers of the acquisition are sent to the RF coil transmitting the excitatory temporally-varying gradients. These coils are designed to provide a fast field switching, with fast rise-times, which enables specificity in the selection of the volume of interest and low-level of distortion in the

magnetic field. The RF coils generate the gradients along three different directions, orthogonal to each other. In brain imaging, extra coils, to be put around the subject's head, can be used to more accurately define the volume of interest (Giussani et al. 2010).

1.4 Brain Activation and Blood Oxygen Level Dependent (BOLD) Effect

The major breakthrough for the application of MRI to the study of brain function was achieved in the early 1990's by Ogawa and colleagues, with the discovery of the blood oxygenation level-dependent (BOLD) contrast (S. Ogawa et al. 1992). This technique, sensitive to local fluctuations in the metabolic and vascular properties of living tissues, allowed for the non-invasive monitoring of human brain function with unprecedented spatial resolution (Seiji Ogawa, Lee, and Barrere 1993). The BOLD effect is the signal change observed due to the change in blood oxygenation in response To localized neuronal activity (S. Ogawa et al. 1993). The timescale of the BOLD response is on the order of seconds after the neuronal activation, which results in a low functional temporal resolution. BOLD contrast relies on the use of hemoglobin (Hb) as an endogenous contrast agent. Hb is the protein, characterized by the presence of an iron molecule, responsible of carrying oxygen in the red blood cells. Depending on its level of oxygen saturation, Hb presents different magnetic properties, in particular, diamagnetic and paramagnetic, when Hb is oxygenated and deoxygenated respectively. Commonly speaking, diamagnetic materials weakly interact with a magnetic field, while paramagnetic substances typically induce distortion in the surrounding magnetic field. When neurons are activated their demand of oxygen increases, thus Hb releases oxygen more easily and changes its state from oxygenated to deoxygenated, and, subsequently, also its magnetic susceptibility. The high-level of deoxy-hemoglobin induces a distortion in the magnetic field inside the MR scanner. This distortion can be detected and interpreted has a measure of the neuronal activity in a certain brain area (Seiji Ogawa et al. 1990). In detail, the distortion of the magnetic field leads to a change of the relaxation time constant $T2*$ in the activated areas, and, therefore, to a difference of the signal intensity in the collected images. It has also been shown that the BOLD response appears with a certain delay, a few seconds, after the neuronal activation (Silva et al. 2000). In fact, changes in blood flow, provoked by the growing metabolic request of the activated neuronal populations, occur over a much slower timescale (hundreds of milliseconds to seconds) than changes in electrophysiological activity (milliseconds or tens of milliseconds) (Silva et al. 2000).

2. SENSORY-MOTOR INTEGRATION

The key to human interaction with the environment lies in the planning and execution of motor movements that coordinate body movements that are in any case necessary for everyday actions over objects. The success of such movements depends on the coordination of several complex factors, including visual cues, tactile and cutaneous feedback, grip force control, and internal representations that control the magnitude, speed, direction, and duration of the force applied to an object's surface.

2.1 Motor Cortex

The upper motor neurons in the cerebral cortex reside in several adjacent and *highly interconnected* areas in the *frontal lobe*, which together mediate the planning and initiation of complex temporal sequences of voluntary movements. These cortical areas all receive regulatory inputs from the *basal ganglia* and *cerebellum* via relays in the ventrolateral thalamus, as well as inputs from the somatic sensory regions of the *parietal lobe*. The motor cortex can be divided into three areas:

1. **Primary motor cortex**. This is the main contributor to generating neural impulses that pass down to the spinal cord and control the execution of movement. It can be distinguished from the adjacent premotor areas both *cytoarchitettonically* (Brodmann's area 4) and by the low intensity of current necessary to elicit movements by electrical stimulation in this region. However, some of the other motor areas in the brain also play a role in this function. It is located in the *precentral gyrus*.
2. **Premotor cortex**. It is responsible for some aspects of motor control, possibly including the preparation for movement, the sensory guidance of movement, the spatial guidance of reaching, or the direct control of some movements with an emphasis on control of proximal and trunk muscles of the body. Located anterior to the primary motor cortex
3. **Supplementary motor area** (SMA). It has many functions including the internally generated planning of movement, the planning of sequences of movement based on prior experience, and the coordination of the two sides of the body such as in bi-manual coordination. Located on the midline surface of the hemisphere anterior to the primary motor cortex. It can be also divided into:
    - **Posterior parietal cortex**. It is sometimes also considered to be part of the group of motor cortical areas; however, it is best to regard it as an association cortex rather than motor. It is thought to be responsible for transforming multisensory information into motor commands, and to be responsible for some aspects of motor planning, in addition to many other functions that may not be motor-related.

- **Primary somatosensory cortex**. Especially the part called Brodmann's area 3a, which lies directly against the motor cortex, it is sometimes considered to be functionally part of the motor control circuitry.

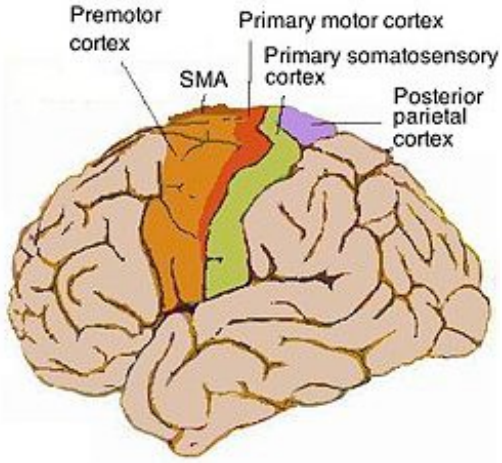

Figure 5. Representation of motor area divided for colors

Motor regions of the cortex and brainstem contain upper motor neurons that initiate movement by controlling the activity of local circuit and lower motor neurons in the brainstem and spinal cord. There are two additional regions of the brain that are important in motor control: the cerebellum and the basal ganglia. They influence movement by regulating the activity of upper motor neurons,

2.2 Cerebellum

The cerebellum can be subdivided into three main parts based on differences in the source of input. As a rule of thumb, each term is constituted by the suffix *–cerebellum* and the prefix indicating the source of input signals:

1. **Cerebrocerebellum.** It is the larger of the three subdivisions and is concerned with the regulation of highly skilled movements, especially the planning and execution of complex spatialized temporal sequences of movement, including speech.
2. **Vestibulocerebellum**. As the phylogenetically oldest part of the cerebellum, this portion comprises the caudal lobe of the cerebellum and includes the flocculus and the nodulus. As suggested by the name, the vestibulocerebellum receives inputs from the vestibular nuclei in the brainstem, and is primarily concerned with the regulation of movements, underlying posture and equilibrium.
3. **Spinocerebellum**. It occupies the median and paramedian zone of the cerebellar hemispheres and is the only part that receives input directly from the spinal cord. The lateral part of the spinocerebellum is primarily concerned with movement of distal muscles, such as relatively gross movements of the limbs during walk. The central part, called the vermis, is primarily

concerned with movements of proximal muscles, and also regulates eye movements in response of vestibular inputs.

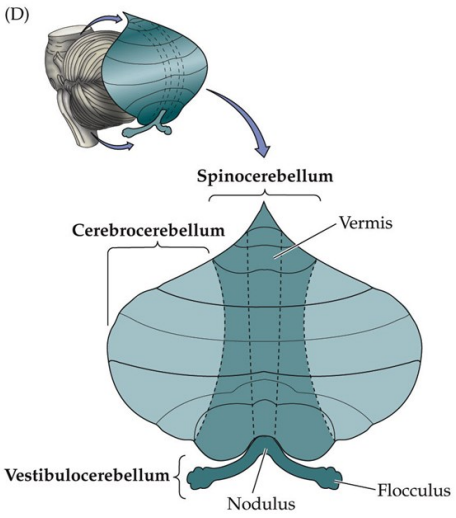

Figure 6. Representation of Cerebellum division

2.3 Basal Ganglia

The basal ganglia are essential to motor control in ways entirely different from those of the cerebellum. Their most important functions of basal ganglia are:

1. To help the cortex execute subconscious but *learned patterns of movements*.
2. To help planning multiple parallel and sequential patterns of movements that brain must put together to accomplish a purposeful task.

On the other hand, the is more addressed to keep muscle tonus and force, correct and stabilize movements by means of feed-forward signals, rapidly initiate a movement, program complex movements, memorize learned movements.

The motor components of the basal ganglia, together with the substantia nigra and the subthalamic nucleus, effectively make a subcortical loop that links most areas of the cortex with upper motor neurons in the primary motor and premotor cortex and in the brainstem. The neurons in this loop respond in anticipation of and during movements, and their effects on upper motor neurons are required for the normal course of voluntary movements.

When one of these components of the basal ganglia or associated structures is compromised, the patient cannot switch smoothly between commands that initiate a movement and those that terminate the movement.

The disordered movements that result can be understood as a consequence of abnormal upper motor neuron activity in the absence of the supervisory control normally provided by the basal ganglia.

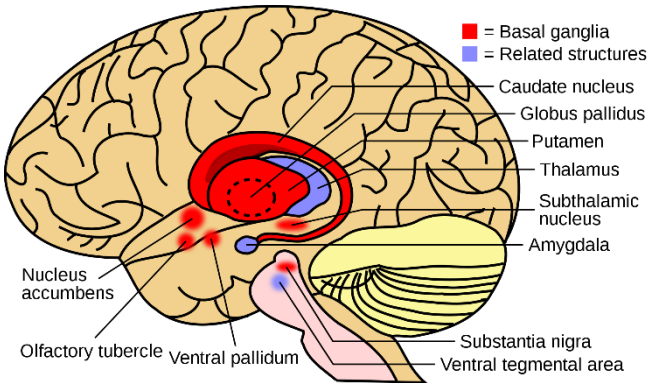

Figure 7. Representation of Basal Ganglia components

In addition to their well-known role in skeletal movements, the basal ganglia control saccadic eye movements (saccades) by means of their connection to the superior colliculus (SC). The SC receives convergent inputs from cerebral cortical areas and the basal ganglia. To make a saccade to an object purposefully, appropriate signals must be selected out of the cortical inputs, in which the basal ganglia play a crucial role. This is done by the sustained inhibitory input from the substantia nigra pars reticulata (SNr) to the SC. This inhibition can be removed by another inhibition from the caudate nucleus (CD) to the SNr, which results in a disinhibition of the SC. (Hikosaka, Takikawa, and Kawagoe 2000)

2.4 Visuomotor integration

Neuroimaging studies have detected the importance of sensory feedback, which plays a fundamental role in accurate motor control in everyday life. The bilateral visuo-parietal-motor network is responsible for the fine control of hand movements, so while the primary motor cortex contralateral to movement (cM1) plays a dominant role in this control, demonstrating convergence support the idea that the ipsilateral primary motor cortex (iM1) also contributes directly to fine hand and finger movements. Similarly, when visual feedback is available, the primary visual cortex (V1) and its interactions with the motor network also become important for accurate motor performance. (Porcaro, Mayhew, and Bagshaw 2021)

An optimized, feedback loop integrates visual information into the motor commands which link the primary motor cortex activity to the limb physics subtending motor behavior. Such transformations are mediated by the dominant, dorsal-stream, visuomotor pathway (Goodale and Milner 1992), which is distinct from the pathways of somatosensory proprioception (Lam and Pearson 2002).

Visual feedback is necessary to detect errors in performance relative to the target. These errors serve as information to revise the motor plan and improve the performance of subsequent trials (Gordon and Ghez 1987). Without it, the user might feel the experience is inconsistent and be unsure about

what triggered a specific action. The ability of visual-motor integration, therefore. Allows visual information to integrate with the information of the gross and fine motor system: the gross motor allows to integrate the visual aspects with the movement of the body while the fine-motor integrates the visual aspects with the hand (hand-eye coordination) and with the graphic aspect.

Furthermore, the systems that control eye movements have a lot in common with the motor systems that regulate the movements of other parts of the body. Just as the spinal cord provides the basic circuits to coordinate the actions of the muscles around a joint, the reticular formation of the pons and midbrain provides the basic circuits that mediate eye movements. The descendant projections from higher-order centers in the superior colliculus and frontal field innervate the gaze centers of the brain stem, providing a basis for integrating eye movements with a variety of sensory information indicating the position of objects in space. The superior colliculus and the frontal visual field are organized in a parallel and hierarchical way, devising one of these structures to compensate for the loss of the other. Eye movements, like other movements, are also under the control of the basal ganglia and cerebellum; this check guarantees the correct start and the correct execution of these simple ones motor behaviors, so observers can efficiently interact with the universe things that can be seen.

3. FUNCTIONAL CONNECTIVITY NETWORKS

3.1 Functional Connectivity

The brain is a very complex organ composed of anatomically specific but highly interconnected regions. Although it accounts for only about 2% of the normal body weight, it consumes about 20% of the total energy (Gillebert and Mantini 2013) . Remarkably, its metabolism is largely constant across time, notwithstanding widely varying levels of cognitive and sensory activity. The complex connectional architecture of the brain and its large energy budget suggest that this organ does not passively analyze and respond to environmental stimuli but actively maintains ongoing representations of cognitive states and behavioral responses, even during idle moments (Engel, Fries, and Singer 2001). To study spatiotemporal patterns of intrinsic activity, specific neuroimaging data analysis methods are available such as: EEG, MEG that revealed much faster neuronal oscillations showing a high temporal resolution and fMRI that show instead a great spatial resolution. These are typically referred to as functional connectivity methods, where functional connectivity indicates statistical interdependence of activity in distant brain regions (Friston 2011).

Functional connectivity is defined as the temporal coincidence of spatially distant neurophysiological events (Friston, 1994). Two regions are believed to show functional connectivity if there is a statistic among the activity measures recorded for them. It is therefore assumed that the areas are coupled or are components of the network if their behavior itself is coherently correlated with each other. Functional connectivity represents a much more direct approach to functional network analysis and agrees with the intuitive notion that when two things happen together, these two things should be related to each other. Relying very little on a priori assumptions, the functional connectivity analysis therefore rather reflects a direct observational measure of functional relationships (Eickhoff and Müller 2015).

When it comes to functional connectivity, we can distinguish between extrinsic and intrinsic functional connectivity:

- Extrinsic functional connectivity: also called functional task-evoked connectivity, it depends on the task performed and therefore on external stimuli
- Intrinsic functional connectivity: measures temporal correlation of spontaneous BOLD signal among spatially distributed brain regions, with the assumption that regions with correlated activity form functional networks.

Functional connectivity analysis, of both fMRI and EEG/MEG data, have documented that intrinsic activity is spatially organized into a finite set of specific, coherent patterns, namely networks.

Functional connectivity can be studied during the performance of active tasks, such as finger tapping or visual stimulation, as well as during resting state, a condition in which the participant is not performing any active task and is simply instructed to remain still, with eyes closed or open while fixating a cross. The simplest and most established approach for constructing RSNs is to extract the time course from a seed region and then determine the temporal correlations between this seed time course and those of all other brain voxels. The resulting correlation map shows the entire network of brain regions having activities similar to that of the seed. Many RSNs are reported in literature such as: visual, auditory, default, dorsal and ventral attention, language and somatosensory networks. Different methods of analysis are developed to implement functional connectivity in both resting and task-related states. We can distinguish them in two main parts: model-based methods and data-driven one. The first one requires a great knowledge and experience in neuroscience because it based on a selection of a region of interest ROI to calculate the connection of this seeds with all the other voxels. The data-driven methods instead do not need any prior knowledge to be implemented. One of the most famous approach, in this respect, is the independent component analysis (ICA) ("(PDF) An Extension of The Herault-Jutten Network to Signals Including Delays for Blind Separation" n.d.). It analyses the entire set of fMRI signals to derive a set of components that are maximally independent in the spatial domain. These components are characterized by a representative time course and a spatial map that expresses the relative contribution of the time course to the fMRI data (Gillebert and Mantini 2013). In the current thesis I aimed to investigate connectivity both within and between functional networks involved in the process.

3.1.1 ROI-to-ROI measures

In the ROI-level approach, the nodes are ROIs that comprise tens to hundreds of voxels. An ROI's signal is typically computed by averaging the BOLD signals of its voxels (Stanley et al., 2013). ROIs are usually defined using an anatomical atlas, based on structural MR images or histological investigations (see, e.g., Stanley et al., 2013). The main benefits of the ROI approach are increased signal-to-noise ratio (SNR) and decreased computational cost. Further, one can expect that cognitive functions cover brain areas larger than single voxels (Shen et al., 2013; Wig et al., 2011). Therefore, the ROI approach may characterize true brain activity better than voxels with functionally arbitrary boundaries. However, areas related to cognitive functions may not necessarily match with the anatomical boundaries that define ROIs: The same function may be distributed across multiple anatomical areas, or one anatomical area may contain several functionally distinct subareas (Papo, Zanin, & Buldú, 2014; Stanley et al., 2013). Thus, the main disadvantage of the ROI approach is the possible loss of information that results from averaging signals of voxels that represent different

functions for producing the ROI signal (Stanley et al., 2013). ROI-to-ROI Correlation (RRC): RRC matrices represent the level of functional connectivity between each pair of ROIs. RRC is defined as the Fisher-transformed bivariate correlation coefficients between two ROIs (Regions Of Interest) BOLD timeseries (ROI BOLD timeseries are computed by averaging voxel timeseries across all voxels within each ROI). Alternatively, bivariate regression coefficient (raw) between the same timeseries:

$$r(i,j) = \frac{\sum_t R_i(t) R_j(t)}{\sqrt{\sum_t R_i(t)^2 \sum_t R_j(t)^2}} \tag{3.1}$$

$$Z(i,j) = tanh^{-1} r(i,j) \tag{3.2}$$

with Ri(t) = BOLD timeseries within i-th ROI, centered to zero mean

- r(i,j) = correlation coefficients between i-th and j-th ROIs
- Z(i,j) = Fisher-transformed correlation coefficient

3.1.2 Network (voxel-level) measures

In the functional brain network approach, the brain is depicted as a collection of nodes and links. Each node represents a brain area that is supposed to be functionally homogeneous, and links represent anatomical or functional connections between nodes. In the voxel-level approach, the nodes are voxels, cubical volume elements with 2–8 mm edges that form a regular grid covering the brain. Intrinsic Connectivity (IC) maps represent a measure of network centrality at each voxel, characterized by the strength of connectivity between a given voxel and the rest of the brain. IC is defined as the root mean square of correlation coefficients between each individual voxel and all of the voxels in the brain (Martuzzi et al. 2011):

$$IC(x) = \sqrt{\frac{\sum_{y \epsilon M} r(x,y)^2}{N}} \tag{3.3}$$

with r(x,y) = correlation coefficients between voxels x and y

• N = number of voxels in analysis mask M

• IC(x) = Intrinsic Connectivity at voxel x

ICA maps represent a measure of different networks expression and connectivity at each voxel, characterized by the strength and sign of connectivity between a given network timeseries and the rest of the brain. It is defined as the multivariate regression coefficients between each component/network timeseries and an individual voxel BOLD timeseries (Nieto-Castanon 2021).

3.2 Independent component analysis (ICA)

ICA is a promising examination technique that is progressively applied to fMRI information. A chief benefit of this approach is its pertinence to mental standards for which point by point models of mind action are not accessible. ICA has been effectively used to dissect single-subject fMRI informational indexes, and an augmentation of this work is accommodate bunch inductions information (Calhoun et al. 2001). ICA endeavors to isolate free "sources" that have been combined as one (blind source division BSS). ICA as applied to fMRI information can be utilized to isolate either spatially and transiently free sources, giving as results spatial and worldly guides of the Independent parts (Ics).

3.2.1 Independent Component Analysis: Algorithms and Applications

Imagine that you are in a room where two people are speaking simultaneously (Hyvärinen, Hyvärinen, and Oja 1999). You have two microphones, which you hold in different locations. The microphones give you two recorded time signals, which we could denote by $x_1(t)$ and $x_2(t)$ with x_1 and x_2 the amplitudes, and t the time index. Each of these recorded signals is a weighted sum of the speech signals emitted by the two speakers, which we denote by s_1(t) and s_2 (t). We could express this as a linear equation:

$$x_1(t) = a_{11}s_1 + a_{12}s_2 \tag{3.4}$$

$$x_2(t) = a_{21}s_1 + a_{22}s_2 \tag{3.5}$$

where a_{11} , a_{12}, a_{21}, and a_{22} are some parameters that depend on the distances of the microphones from the speakers. It would be very useful if you could now estimate the two original speech signals s_1(t) and s_2 (t), using only the recorded signals $x_1(t)$ and x_2 (t). This is called the cocktail-party problem. As an illustration, consider the waveforms in Figure 7 and Figure 8.

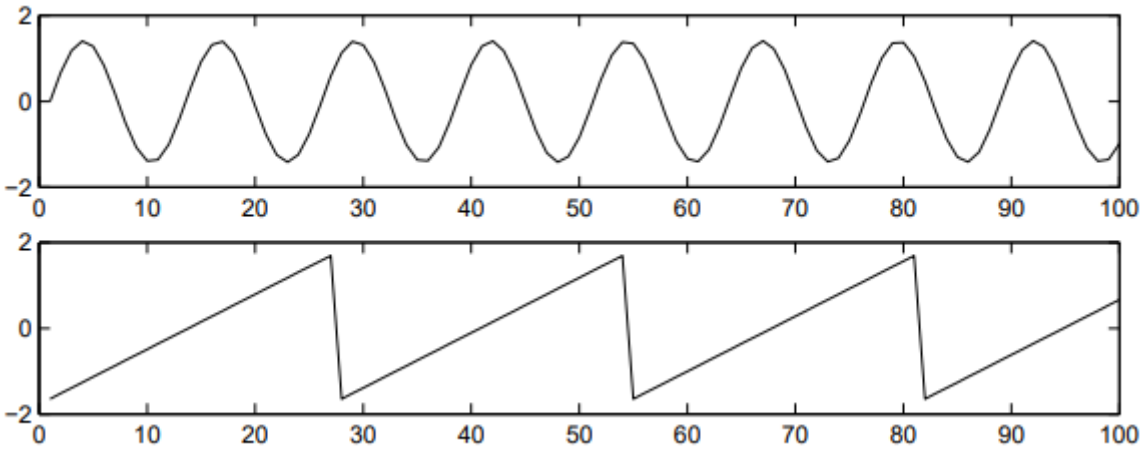

Figure 7. The original signals

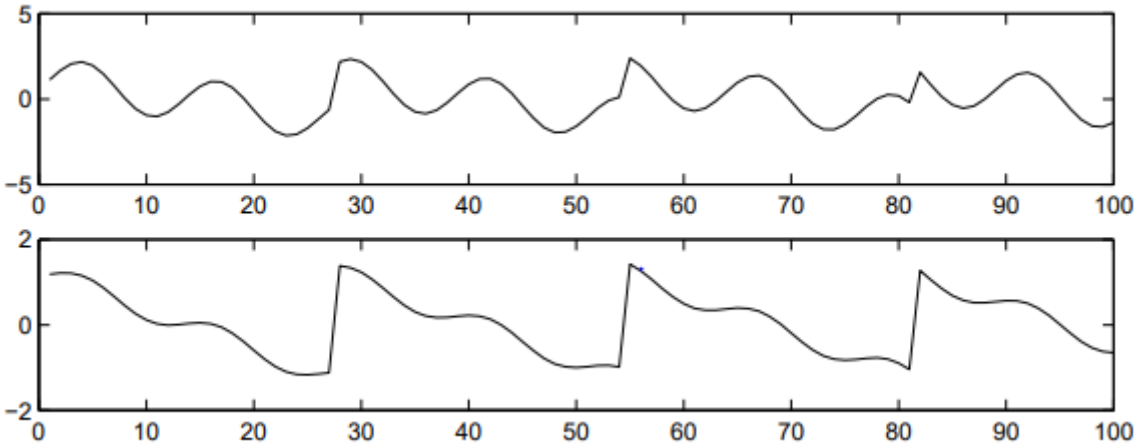

Figure 8. The observed mixtures of the source signals in Fig.7

These are, of course, not realistic speech signals, but suffice for this illustration. The original speech signals could look something like those in Fig. 7 and the mixed signals could look like those in Fig. 8. The problem is to recover the data in Fig. 7 using only the data in Fig. 8. Actually, if we knew the parameters a_{ij} , we could solve the linear equation in (1) by classical methods. The point is, however, that if you don't know the a_{ij} , the problem is considerably more difficult. One approach to solving this problem would be to use some information on the statistical properties of the signals $s_i(t)$ to estimate the a_{ii} . Actually, and perhaps surprisingly, it turns out that it is enough to assume that $s_1(t)$ and $s_2(t)$, at each time instant t, are statistically independent. This is not an unrealistic assumption in many cases, and it need not be exactly true in practice. The recently developed technique of Independent Component Analysis, or ICA, can be used to estimate the a_{ij} based on the information of their independence, which allows us to separate the two original source signals $s_1(t)$ and $s_2(t)$ from their mixtures $x_1(t)$ and $x_2(t)$. Fig. 9 gives the two signals estimated by the ICA method. As can be seen, these are very close to the original source signals (their signs are reversed, but this has no significance).

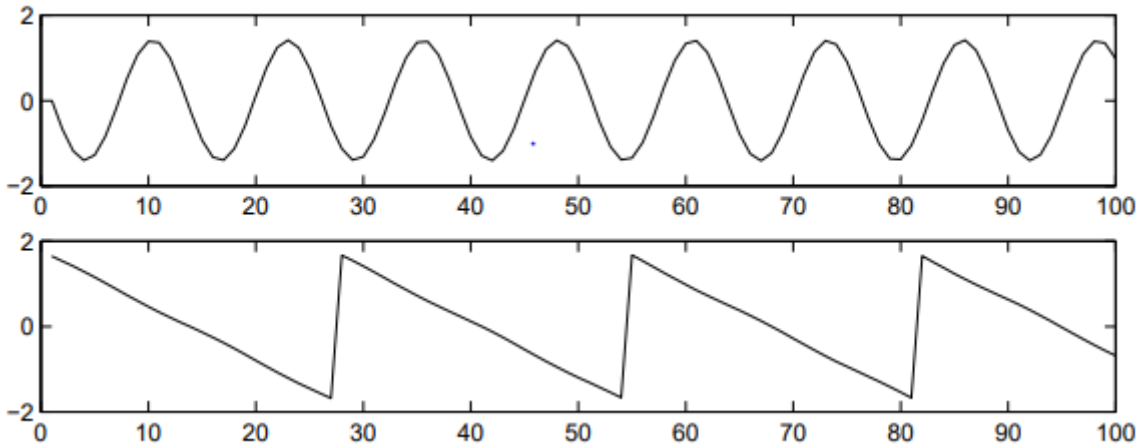

Figure 9. The estimates of the original source signals, estimated using only the observed signals in Fig. 8. The original signals were very accurately estimated, up to multiplicative signs.

3.2.2 *Definition of ICA*

To rigorously define ICA (Nomura et al. 1996) we can use a statistical "latent variables" model. Assume that we observe n linear mixtures $x1,...,xn$ of n independent components

$$x_j = a_{j1}s_1 + a_{j2}s_2 + \cdots + a_{jn}s_n, for\ all\ j. \tag{3.6}$$

We have now dropped the time index t; in the ICA model, we assume that each mixture x_j as well as each independent component s_k is a random variable, instead of a proper time signal. We have now dropped the time index t; in the ICA model, we assume that each mixture x_j as well as each independent component s_k is a random variable, instead of a proper time signal.

The observed values x_j (t), e.g., the microphone signals in the cocktail party problem, are then a sample of this random variable. Without loss of generality, we can assume that both the mixture variables and the independent components have zero mean: If this is not true, then the observable variables xi can always be centered by subtracting the sample mean, which makes the model zero-mean. It is convenient to use vector-matrix notation instead of the sums like in the previous equation. Let us denote by **x** the random vector whose elements are the mixtures $x_1,...,x_n$, and likewise by **s** the random vector with elements $s_1,...,s_n$. Let us denote by **A** the matrix with elements a_{ij}. Generally, bold lower-case letters indicate vectors and bold upper-case letters denote matrices. All vectors are understood as column vectors; thus $\boldsymbol{x^T}$**,** or the transpose of **x**, is a row vector. Using this vector-matrix notation, the above mixing model is written as:

$$x = As \tag{3.7}$$

Sometimes we need the columns of matrix **A**; denoting them by $\boldsymbol{a_j}$ the model can also be written as

$$x = \sum_{t=1}^{n} a_j s_j \tag{3.8}$$

The statistical model in Eq. 4 is called independent component analysis, or ICA model. The ICA model is a generative model, which means that it describes how the observed data are generated by a process of mixing the components s_j. The independent components are latent variables, meaning that they cannot be directly observed. Also, the mixing matrix is assumed to be unknown. All we observe is the random vector **x**, and we must estimate both **A** and **s** using it. This must be done under as general assumptions as possible. The starting point for ICA is the very simple assumption that the components s_i are statistically independent. The independent component must have *nongaussian* distributions. For simplicity, we are also assuming that the unknown mixing matrix is square. Then, after estimating the matrix **A**, we can compute its inverse, say **W**, and obtain the independent component simply by:

$$s = Wx \tag{3.9}$$

ICA is very closely related to the method called blind source separation (BSS) or blind signal separation. A "source" means here an original signal, i.e. independent component, like the speaker in a cocktail party problem. "Blind" means that we know very little, if anything, on the mixing matrix, and make little assumptions on the source signals. ICA is one method, perhaps the most widely used, for performing blind source separation.

3.3 Main Network

Large-scale brain networks (also known as intrinsic brain networks) are collections of widespread brain regions showing functional connectivity by statistical analysis of the fMRI BOLD signal. Through functional connectivity, the main large-scale brain networks have been identified, having the greatest function over the cortex in the brain and each performing a general function. These major networks control brain function both during task processing and while at rest.

Depending on the granularity of how a network is defined, there is no single number of brain networks but at the highest level, the brain can be thought to consist of seven main networks – sensorimotor system, visual system, limbic system, central executive network (CEN), default mode network (DMN), salience network and dorsal attention network (DAN).

The brain's neural networks have a hierarchy to their operation, and they integrate and synchronize to carry out "complex functions."

The nodes of these core networks have been inferred from the results of fMRI studies, during tasks that manipulate one or more of these cognitive functions. A full characterization of core functional brain networks, however, will require additional studies to validate the nodes of these networks using other criteria, to measure their edges, and to determine whether other core networks exist. In this thesis were investigate main networks involved in a particular visuomotor task and its relations has been used. The results obtained for this thesis confirm results obtained in other studies and add information on the brain regions involved in our task showing that visual network, sensorimotor network, Default mode network, attention network, cerebellum, basal ganglia are the main networks underlying sensorimotor actions.

3.3.1 Default mode network

The default mode network (DMN) is the "internal mind." When the brain is in a resting state and isn't actively engaged in focused, goal-oriented tasks, "default" or subconscious brain activity increases

for internal thought processing, (Raichle et al. 2001)which likely evolved from evolutionary self-preservation.

Since we are nearly always thinking to ourselves or subconsciously processing the world around ourselves, the DMN is considered the most active and consistent (Lee et al. 2012) of the seven main brain networks.

Due to its frequent activity, DMN plays an integral role in coordinating with other networks for passive sensory processing.(Greicius et al. 2003) These connections often include:

- Visual processing in conjunction with the visual system when the mind subconsciously appreciates aesthetic beauty, (Vessel et al. 2019) like when observing impressive artwork or architecture.
- Semantic processing (Wirth et al. 2011) with the language subnetwork when encoding or translating meaning into spoken or written words.
- Processing or evaluating personal emotions or the emotions of others, with the limbic system. (Raichle et al. 2001)

Very important, when talking about this network, is its interaction with the Executive Control Network since the previous study indicated that the areas of the DMN remain uniformly active in a waking state but at rest, (Raichle et al. 2001)and there is a decrease of this activity when other brain areas become active for goal-related tasks or for the response to external stimuli.1 Through this study, neurologists determined that the brain's activity switches between the DMN's internal state and an external processing state in the central executive network (CEN). Together, these two networks are considered the brain's dominant control networks.

Most importantly, the control networks occur in counterbalance to one another. As soon as the CEN switches into high gear for active and external task processing, the DMN is deactivated. (Ekhtiari et al. 2016) The salience network is responsible for the imperceptible switches back and forth — from introspective thinking to external active tasks and back to internal thought.

The relationship between the DMN and CEN is a critical balance, and the two networks should not be active at the same time. Increased activity in one or both networks has been implicated in multiple mental health disorders.

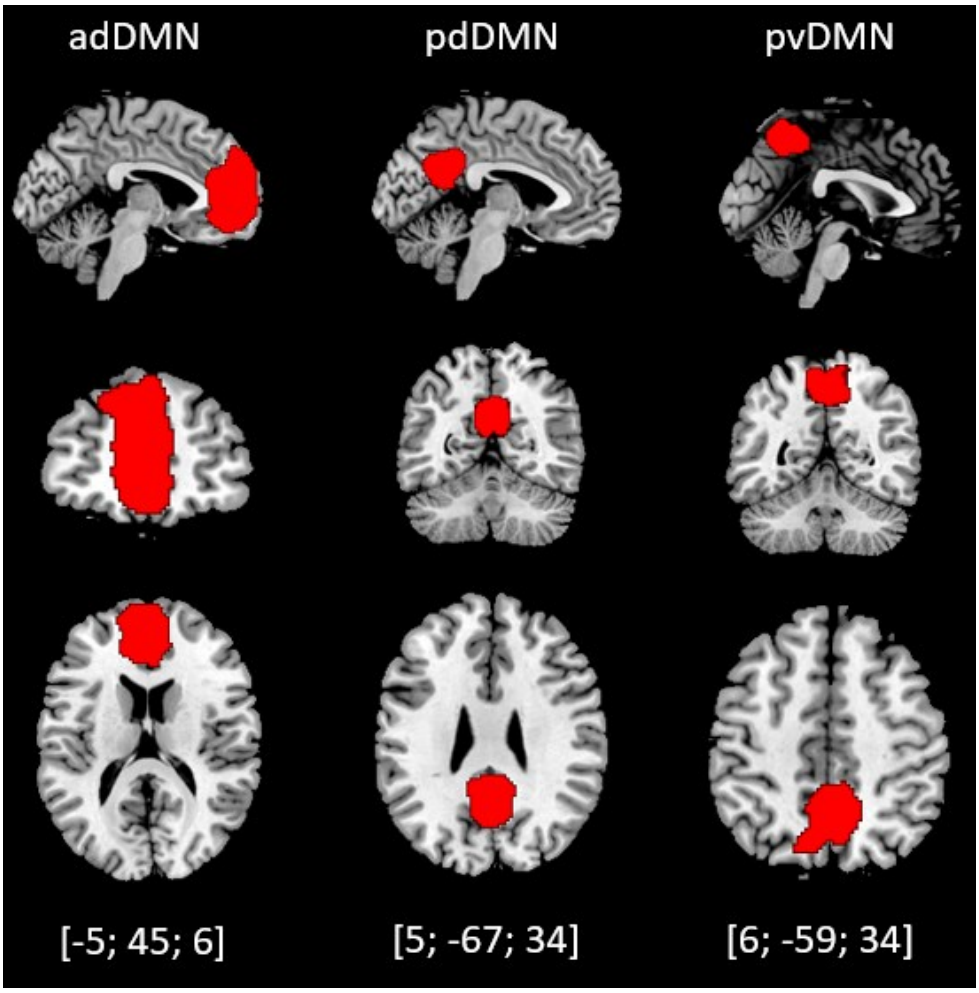

Figure 10. From left to right: Anterior dorsal Default mode network (adDMN), posterior-dorsal DMN (pdDMN) and posterior-ventral DMN (pvDMN). The main core nodes of the DMN showed in the most representative slices.

3.3.2 Attention network

The Attention network comprises Salience Network (SN) and Control Executive Network (CEN). In the past SN and CEN were together considered to comprise ‘’task-positive network’’ or ‘’task-activation ensemble’’. Seeley and colleagues demonstrated two important points in their seminal work (Seeley et al., 2007):

(1) they are two dissociable networks (SN and CEN) critical for guidance of behaviors

(2) intrinsic connectivity of these two networks differentially correlates with individual differences in anxiety and executive task performance.

The salience network (SN) is “the moderator.” As your mind’s personal moderator, the salience network constantly monitors the external world and carefully decides how other brain networks react to new information and stimuli, also regulates and transitions between networks swiftly and imperceptibly to address the changing demands of the moment. 4

The SN moderates switching between the internal and external processing1 of the brain's two main control networks:2 the default mode network (DMN) and central executive network (CEN), respectively.

The salience network also plays a critical role in processing pain, emotion, reward, and motivation3 in connection with the limbic system. In these cases, the moderator decides how much the human body "hears" signals involving emotional response.

Th other network of the AN is the CEN, that performs high-level cognitive tasks, and works alongside or in anticorrelation with the other six main brain networks.

The CEN engages in:

- Active tasks and external thinking involving working memory
- Controlled processing of information
- Integration of information from the other brain networks
- Rule-based problem solving and decision making
- Consideration of multiple, independent stimuli and independent factors
- Organizing behavior based on internal drives, subjective preferences, and choices
- Reinforce visually learned behaviors

Like previously mentioned, the CEN correlates with the DAN for attention processing, as well as visual spatial planning. It has always been said that the CEN and the DMNs worked in opposition, that is, that the activation of one determined the inhibition of the other, and that the SN mediated the activity of these networks due in opposition. Beaty and colleagues, instead, in their (Beaty et al. 2015) reveal that there is a strong connection between DMN and CEN, they work together and not in opposition as it was thought (Beaty et al. 2015).

The central executive network also integrates with each of the other networks as needed for task processing:

- Receives visual inputs from the visual network
- Evaluates auditory inputs from the auditory network
- Receives sensory inputs from the sensorimotor network while also sending back task directives (Niendam et al. 2012)
- Processes stimuli and motivational signals from the limbic system.

Since the CEN interacts so closely with other large-scale brain networks, it has been implicated in many neuropsychiatric disorders.

Aberrant switching between the CEN and DMN as a result of an over- or underactive SN has been demonstrated as a symptom of schizophrenia and post-traumatic stress disorder (PTSD). (Daniels et al. 2010)

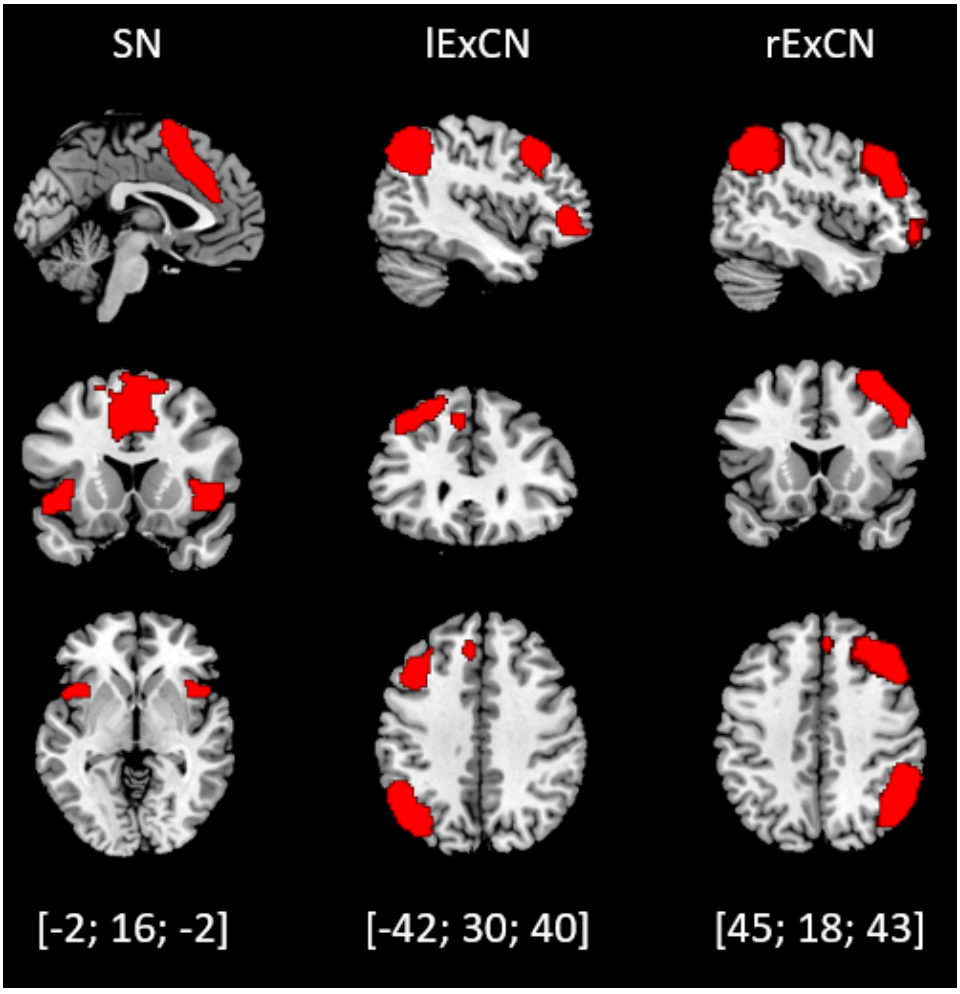

Figure 11 From left to right: Salience Network (SN) Left Executive Control Network (lExCN) Right Executive Control Network (rExCN). Core nodes of the Attention Network showed in their most representative slices.

3.3.3 Sensorimotor Network

The sensorimotor network is "the transducer." As the brain's transducer, the sensorimotor network is responsible for sensing physical inputs, converting them to electrical signals that travel throughout the brain network, and then initiating a physical response

The sensorimotor network is responsible for:

- Processing external physical stimuli
- Feeling internal sensations
- Evaluating the senses

- Producing a motor response.

Because of its importance in daily life, physicians pay special attention to the motor cortex and the primary somatosensory cortex. The primary somatosensory cortex, in collaboration with the secondary somatosensory cortex, processes bodily sensations and sends signals to the motor cortex to execute reactions and appropriate motor responses.

As the brain's transducer, the sensorimotor network works closely with the other main brain networks to carry out key processes. It works alongside the:

- Auditory subnetwork for hearing (Chang et al. 2013)
- Visual system for sight
- Salience network for behavior and reward processing
- Central executive network for task processing (Stevens et al. 2007)
- Dorsal attention network for planning and controlling complex motor functions (Corbetta and Shulman 2002)
- And the default mode network in cases of physical or mental illness

Together, the individual nodes in these systems share functional connections that make up our senses and guide our actions. Yet, they can also lead to mental or physical illness when they become over- or underactive.

Abnormalities in the sensorimotor network can cause sensory and movement disorders, as well as degenerative diseases, developmental delays, and mental health disorders.

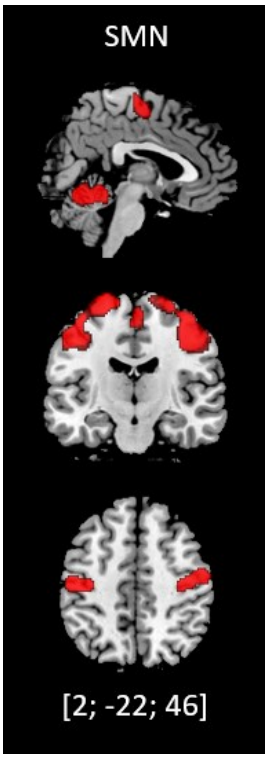

Figure 14 Sensorimotor network (SMN), bilateral activation in their most representative slices.

3.3.4 Visual Network

The visual system controls sight and visual processing, making the system simple to understand even though it handles complicated tasks. It is a very intricate network of components that all work together to transform light into a recognizable form.

The visual system, which at first glance appears to be a single brain region, is actually made up of a number of nearby functional units that cooperate to process visual information cohesively.

Combined, they:

- process images in your mind's eye
- considering motion
- recognize faces, patterns, and textures
- rocalize people, structures, or items in space Identification of the use and permanence of objects
- support problem-solving
- reaffirming habits that have been seen

The multiple nodes that compose this network are functionally and structurally connected as distributed networks that make up the dorsal and ventral pathways.

The visual system works closely with many of the brain's networks:

- Dorsal attention network (DAN) for reading and general visual processing (Vogel et al. 2012)
- Sensorimotor network for early development (Sale et al. 2004) and imitation learning
- Limbic system for visual memory and processing threat-based stimuli noticed in an individual's peripheral vision (Montirosso et al. 2010).
- Salience network for self-control when presented with tempting imagery as well as emotional empathy (Bilevicius et al. 2018)

The interruption of the coordination between the visual network and the other brain networks or the occurrence of problems between the nodes belonging to the network can cause visual impairment and mental health problems.

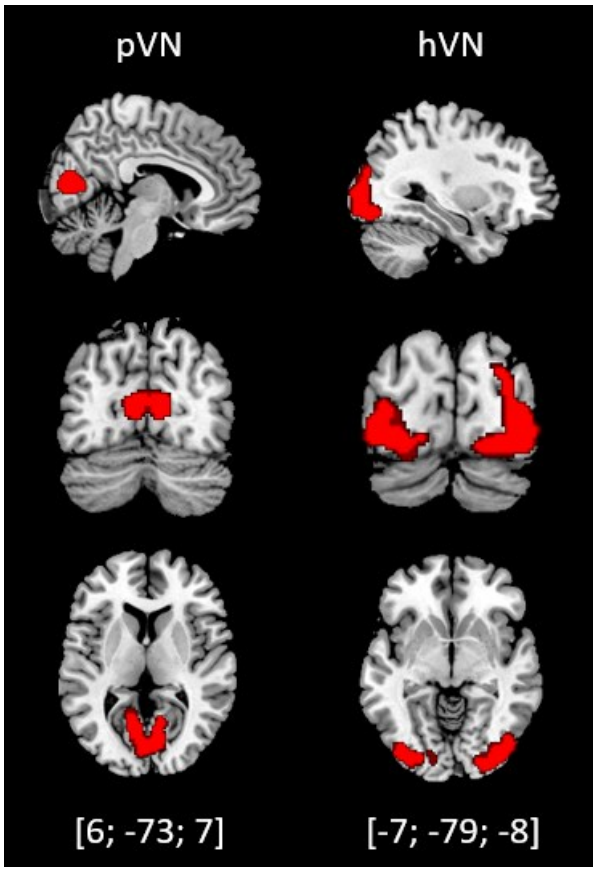

Figure 15 Primary Visual Network (pVN) and High Visual Network (hVN), bilateral activation in their most representative slices.

3.3.5 Frontal Eye Field

The Frontal Eye Field (FEF) is a region of primate prefrontal cortex defined as the area in which low-current electrical stimulation evokes saccadic eye movements. On the basis of stimulation, recording, and inactivation experiments, the FEF appears to play a significant role in the planning and execution of saccadic eye movements. These same types of experiments have more recently demonstrated that the FEF also participates in the control of visual selective attention.

The frontal eye field is reported to be activated during the initiation of eye movements, such as voluntary saccades and pursuit eye movements (Mustari, Ono, and Das 2009). There is also evidence that it plays a role in purely sensory processing and that it belongs to a "fast brain" system through a superior colliculus – medial dorsal nucleus – FEF ascending pathway. FEF has also an important role in the covert allocation of spatial attention through its reciprocal connectivity with visual cortex (Bedini and Baldauf 2021).

The unilateral irritative function of an FEF causes the conjugate, therefore a paralysis, contralateral to the gaze. Conversely, a one-sided destructive lesion of the FEF causes the conjugate gaze towards the lesion.

Figure 17 Frontal Eye Field (FEF) in its most representative slices.

3.3.6 Basal Ganglia

The original functional organization of the basal ganglia was conceived as a loop, in which cortical afferent activity is dispatched to and modulated by the basal ganglia, which subsequently sends back a signal to the cortex to facilitate (or inhibit) motor activity. The basal ganglia were featured as a "go through" station within the motor loop. Current thinking now is that the basal ganglia has several loops, where cortical and subcortical projections interact with internal reentry loops forming a

complex network, ideally designed for selecting and inhibiting simultaneously occurring events and signals. (Lanciego, Luquin, and Obeso 2012)

The basal ganglia, through interactions with the cerebral cortex, contribute to voluntary movement and other forms of behavior such as skeleton-motor, oculomotor, cognitive and emotional functions. In particular in motor control:

1. they guarantee the automatic execution of movements such as walking, running, facilitating the actions controlled by the higher cortical centers (cortex) and suppressing the muscular activities that would prevent their execution
2. They can modify or suppress these activities in new or unforeseen situations (a sudden obstacle) by re-establishing the control exercised by the cortex.

The basal ganglia exert inhibition on motor systems based on signals from many parts of the brain, including the prefrontal cortex, which plays a key role in executive functions.

In addition, the basal ganglia, including the internal pale globe and the subthalamic nucleus, are involved in the processing of reward and motivation.

If the basal ganglia are damaged, some functions, such as the control of voluntary movements, eye control or procedural learning, could also be severely and irreversibly altered. The basal ganglia are extremely important for human sociality: they help decide which of the possible behaviors is most appropriate to perform at a given time based on the circumstances.

Figure 17 Basal Ganglia (BG) in its most representative slices.

3.3.7 Cerebellum

Cerebellum's functions revealing connectivity to motor and nonmotor cerebral areas. Within the motor domain, the cerebellum is seen as supporting the efficient and effective implementation of behavior. Cerebellum controls and coordinates complex movements and is important for adapting movements to changes in feedback. It does not initiate movement, but contributes to coordination, precision, and accurate timing: it receives sensory and motor information from descending cortical pathways and ascending peripheral pathways. It has also connections to the parietal, pre-motor, and frontal cortices. A meta-analysis by Stoodley and Schmahmann revealed that the right hemisphere being more active for language and the left for visuospatial tasks. Peter Mariën and colleagues assessed the role of cerebellum in language associated in terms of structure involved in the "handling" of phonetic timing information. Some studies reveal that the cerebellum is involved during ''executive function'' such as: directing attention, decision making, working memory, but it may not be possible to highlight purely executive cerebellar region (Goel et al. 2000) (STOODLEY and SCHMAHMANN 2009).

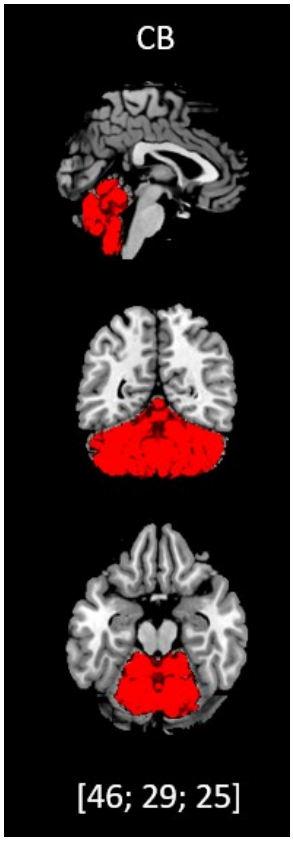

Figure 18 Cerebellar (Cb) network in its most representative slices

4. FMRI CHARACTERIZATION OF INTRINSIC BRAIN NETWORKS RELEVANT FOR MOTOR CONTROL WITH AND WITHOUT VISUAL FEEDBACK BY FRACTAL DIMENSION

4.1 Abstract

The bilateral visuo-parietal-motor network is responsible for fine control of hand movements. However, the subregions devoted to maintaining contraction stability in the presence/absence of visual feedback remain unclear. It is widely recognized that continuous sensory feedback plays a crucial role in accurate motor control in everyday life. Feedback information is used to adapt force output and to correct errors. While the primary motor cortex contralateral to the movement (cM1) plays a dominant role in this control, converging evidence supports the idea that the ipsilateral primary motor cortex (iM1) also directly contributes to hand and finger movements. Similarly, when visual feedback is available, the primary visual cortex (V1) and the visuospatial network and their interactions with the motor network are essential for accurate motor performance. To clarify this problem and investigate the regions involved in a visuomotor task, we performed functional magnetic resonance imaging (fMRI) measurements during isometric compression of a compliant rubber bulb, at 10% of maximum voluntary contraction, both with (visuomotor task) and without visual feedback (motor task).

Here, by using a multivariate approach focusing on intrinsic connectivity between voxels through group ICA of fMRI Toolbox (GIFT), we have answered the following two main questions:

1) which are the networks involved during a motor task (i.e. without visual feedback) and a visuomotor task (i.e. with visual feedback)?

2) Is there any hemodynamic signal complexity difference between the visuomotor and the motor task?

Interestingly, we have found that during the visuomotor task, the involvement of the visuospatial network (FEF), the ipsilateral primary motor area (iM1), the contralateral primary motor area (cM1), the sensorimotor network (SMN) the Executive Control Network (ExCN), the Silence Network (SN), the Default Mode Network (DMN), the Basal Ganglia (BG), the Cerebellum (Cb) and Precuneus are essential for the fine motor control of the movement while maintaining the grip force level indicated by the visual feedback together with higher complexity estimated by Higuchi's Fractal Dimension.

4.2 Introduction

A key component of human interaction with our surrounding environment is the planning and execution of motor actions to coordinate movements of the body. Grasping and manipulation of

objects in a controlled and precise manner is an essential action that depends upon smooth coordination and integration of diverse sensory components such as visual cues, tactile and cutaneous feedback, grip force control and internal representations. (Porcaro, Mayhew, and Bagshaw 2021) The organization of the brain's activity during the coordination of precision or force gripping, using either dynamic or isometric contractions, has been investigated by numerous functional magnetic resonance imaging (fMRI) studies as a foundation for studying more complex motor tasks. This body of work has identified a bilateral fronto-parieto cerebellar network, primarily comprised of primary sensorimotor cortex (M1/S1), dorsal and ventral premotor cortices (PMd and PMv), supplementary and cingulate motor areas (SMA and CMA), prefrontal cortex, parietal association cortex and the cerebellum. (Mayhew et al. 2017)

However, two aspects have been largely neglected by previous studies which, impairing a complete understanding. First, most previous studies have focused on understanding unimanual motor behavior by studying only task activations in cortical, sub-cortical and cerebellar structures. The traditional view has long held that motor execution is lateralized, with the activation of the contralateral primary motor cortex (cM1) playing a dominant role. However, during unimanual motor and somatosensory tasks the activity of ipsilateral M1 (iM1) is neither quiescent nor idling but substantially perturbed by the task, typically in the form of a reduction in mu frequency (8– 13 Hz) M/EEG power or fMRI signal below baseline levels. (Verstynen et al. 2005b; Verstynen and Ivry 2011; Pfurtscheller and Lopes Da Silva 1999; Neuper, Wörtz, and Pfurtscheller 2006) Second, the visual feedback signal control seems to emphasize this aspect, especially during fine movement control. (Porcaro, Mayhew, and Bagshaw 2021)

From a metrological point of view, another key point is that all the studies using fMRI to study motor control and execution have used the mass-univariate voxel-based approach, which focuses on segregating and localizing processes, failing to account for the integration across functions within more extensive networks. In addition, the mass-univariate voxel-based analysis also relies on subtraction methods between conditions, placing greater emphasis on differences then similarities between processes. Functional connectivity analysis is an alternative multivariate method to assess the functional architecture of the central nervous system that integrates brain signals across multiple regions. This approach uses correlations between distant regions as the dependent variable. Independent component analysis (ICA) is often used to identify clusters of regions that show high correlations of signal change within a given time window. These clusters are assumed to reflect intrinsic connectivity networks. Consistent intrinsic networks have been repeatedly identified using ICA. These include networks that connect homologous regions processing visual, auditory, and sensory-motor output. But also, higher cognitive function (Marino et al. 2019) such as the default

mode network (anterior and posterior midline and inferior parietal); the lateralized dorsal frontal-parietal network, putatively involved in attention; the saliency network which comprises the insula and the anterior cingulum; the frontal network involving prefrontal, frontotemporal, and cingulate cortex, thought to reflect executive control; the left-lateralized ventral, frontal, and parietal network, involved in language processing and the precuneus, basal ganglia, and a cerebellum network. Importantly, similar networks are detected when participants are engaged in a task (goal-driven behavior). In addition, differences between specific task conditions are modelled as a reconfiguration of connections within and between networks. It has been argued that the task-based spatial ICA data-driven approach is advantageous over conventional mass-univariate analysis of signal amplitude change. This is because it does not rely on assumptions regarding the time course, the temporal characteristics, and the shape of the hemodynamic response function.

In this thesis, we analyzed fMRI data recorded from sixteen healthy volunteers (Mayhew et al. 2017) using a multivariate data-driven approach focusing on intrinsic connectivity between voxels through group ICA of fMRI Toolbox (GIFT), asking the following main questions:

1. which are the networks involved during a motor task (i.e. without visual feedback) and a visuomotor task (i.e. with visual feedback)?

2. Is there any hemodynamic signal complexity difference between the visuomotor and the motor task and in which brain networks?

We have answered these two questions by recording the hemodynamic brain activity by fMRI technique in sixteen healthy right-handed volunteers during a motor (M - i.e. without visual feedback) and visuomotor (VM - i.e. with visual feedback) task performed by an isometric contraction by squeezing a semi-compliant rubber bulb with their right hand.

4.3 Material and method

4.3.1 Partecipants

Sixteen right-handed volunteers (age = 26±4 years, 7 females) performed an isometric contraction of a pneumatic rubber bulb (Van Wijk et al. 2009) opposing the thumb to the first two fingers of their right-hand. Handedness of every subject was assessed using the Edinburgh handedness inventory, group mean ± standard deviation = 91.8 ± 14.1. Written informed consent was obtained from all participants and the protocol was approved by the Research Ethics Board of the University of Birmingham.

4.3.2 Experimental Paradigm

Individual's maximal voluntary contraction (MVC) of this grip was measured prior to the experiment using a mechanical hand dynamometer (0–100 kgs, Lafayette 78010, Indiana). Three trials were performed where subject's held maximum contraction for 5 s and the mean force value across trials was used as their MVC. The pneumatic device enabled the accurate measurement of contraction force, thus enabling task performance to be quantified. An increase in the contraction force applied to the rubber bulb increased the pneumatic pressure inside a rubber tube, which was translated into an analogue electrical signal by in-house electronics and recorded by a Ni-DAQ (National Instruments) (Van Wijk et al. 2009). Prior to the experiments, the pneumatic equipment was calibrated so that the conversion of applied force to current was known. The contraction force was continuously recorded throughout all experiments at 100 Hz sampling rate.

During the experiment, subjects were instructed to maintain the isometric contraction for the 5-second trial duration 10% of MVC. Throughout the experiment subjects viewed a visual display, which was projected onto a screen situated behind them at the rear of the scanner bore, via a mirror mounted on the MRI headcoil. Subjects kept their eyes open at all times and maintained fixation upon a vertical, white force-gauge that was centrally displayed upon a grey background throughout. The position of the segments aside the gauge indicated the required force (i.e. the 10% MVC), and their appearance communicated the onset of each trial (Fig. 19).

Subjects were instructed to smoothly increase the contraction force and to then maintain this target force level as accurately as possible until the end of the trial, signaled by the disappearance of the two segments aside the gauge. At the trial offset, subjects were instructed to terminate the contraction and completely relax their hand for the duration of the inter-stimulus interval lasting either 5, 7 or 9 s. The choice of task durations was motivated by ensuring a stable and reliable contraction period; secondly that we recorded a sufficient number of trials, for both 10% condition, to allow meaningful correlations between fMRI responses and single-trial performance to be calculated, without creating an over-long total experimental duration. Isometric contractions at the force levels were executed in two experimental conditions (see Fig. 16 for a schematic representation of the task display):

1) Visuomotor condition (VM), where a horizontal, black force indicator bar appeared centrally in the force gauge upon trial onset. The vertical position of this horizontal indicator provided continuous visual feedback information to the subject about the exerted contraction force (Fig.19 B). The force indicator was removed from the visual display at trial offset.

2) Motor condition (M), where subjects were asked to perform the isometric contraction without the display of the horizontal force indicator (Fig.19 C).

Although matching the target force level was obviously more difficult in this M-task, subjects had been familiarized with the task during a single-run of each of the tasks conducted outside of the MRI scanner immediately before the fMRI experiment and were reasonably competent at performing the task at the required force levels.

Experimental cues were visually presented to participants via a projector display and the visual display was controlled using the Psychophysical toolbox running in MATLAB (MathWorks). Immediately before fMRI scanning each subject performed a practice run of the VM and M tasks to familiarize them with the task and eliminate learning effects.

During fMRI, two experimental runs of each of the VM- and M-task conditions were acquired in an inter leaved order that was randomized across subjects.

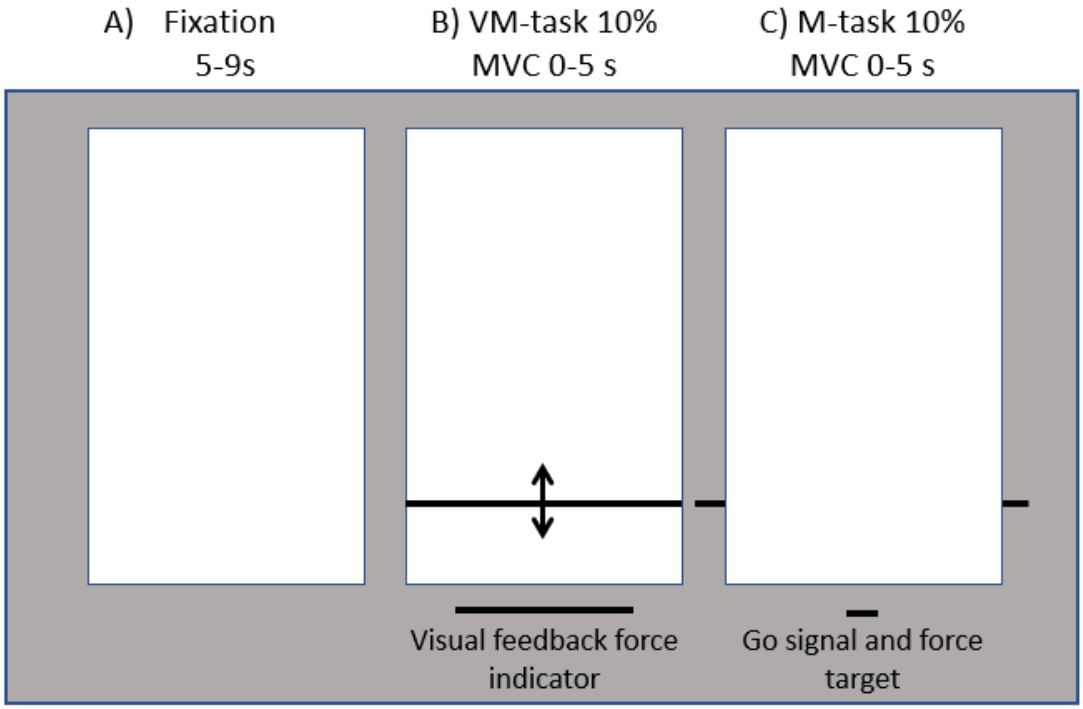

Figure 19. Experimental conditions. Illustration of the visual display during the task conditions. A rectangular white force gauge was displayed throughout all runs of the experiment and served as the resting fixation condition (A) during the 5, 7 or 9 s inter-stimulus interval. The visual display during the whole 5 s duration of the visuomotor feedback (VM) task of the MVC10% (B) and motor (M) task 10% of the MVC (C) contractions are also shown. The trial onset GO signal was provided by the appearance of the two black side-bars instructing the target force level required in each trial. In the VM-task only, a horizontal black bar indicating the current contraction force was also displayed from trial onset. This force indicator bar moved vertically up/down the screen when the subject exerted greater/lesser force to provide real-time visual feedback of task performance. The movement of the indicator bar is illustrated in the figure using dashed line arrows that were not displayed during the experiment.

4.3.3 fMRI data acquisition

All experiments were conducted at the Birmingham University Imaging Centre using a 3T Philips Achieva MRI scanner. An eight channel phased-array head coil was used to acquire T1-weighted

anatomical image (1 mm isotropic voxels) and four task-related whole-brain T2*-weighted, functional EPI data (365 volumes, 3x3×4 mm voxels, 32 slices, TR=2000 ms, TE=35 ms, SENSE factor=2, flip angle=80°). Cardiac and respiratory cycles were continuously recorded (pulse oximeter and respiratory belt

4.3.4 fMRI Pre-processing and analysis

4.3.4.1 fMRI analysis by Statistical Parametric Mapping (SPM-Toolbox)

The fMRI data were analyzed using SPM12 (Wellcome Department of Imaging Neuroscience, London; https://www.fil.ion.ucl.ac.uk/spm/). Pre-processing of the data included slice time correction, spatial realignment to correct for movement artefacts and motion by distortions interactions and normalized to the MNI standard space. The data were re-sampled given a 2x2x2 voxel size and smoothed using 6 FWHM Gaussian Kernel to account for residual inter-subject differences and to accommodate assumptions of random field theory used for family wise error corrections. We first estimated the effect size for each participant on each of the four conditions (recall 2x2 design) using the general linear model. Each condition was modelled by a separate regressor; the onsets of each trial corresponded to the time when a correct response was given. All the regressors were convolved with three bases functions: the canonical HRF, its derivatives and dispersions. To correct for signal changes due to head movement, the 6 realignment parameters were included in the design matrix. An additional set of regressors was added for force contraction.

4.3.4.2 fMRI analysis by Group ICA of fMRI Toolbox (GIFT)

Data were decomposed into functional networks using a group-level spatial ICA as implemented in the GIFT toolbox (https://trendscenter.org/software/gift/). The individual datasets were temporally concatenated and reduced for computational feasibility through three stages of principal component analysis (PCA) in order to reach the final dataset, which was then decomposed by ICA with Infomax (Bell and Sejnowski 1995) algorithm into 100 (ICs=100) spatially independent components.

In GIFT, after each subject's functional data were reduced, the data were then concatenated into groups and put through another data reduction step. The number of subjects to put into each group is called partitions with the number of datasets in a partition being equal to the one-fourth of the number of data-sets selected for. After reduction within each partition the data were stacked into one group and put through the final data reduction. At this stage, the number of components was estimated using the minimum description length criteria (MDL).

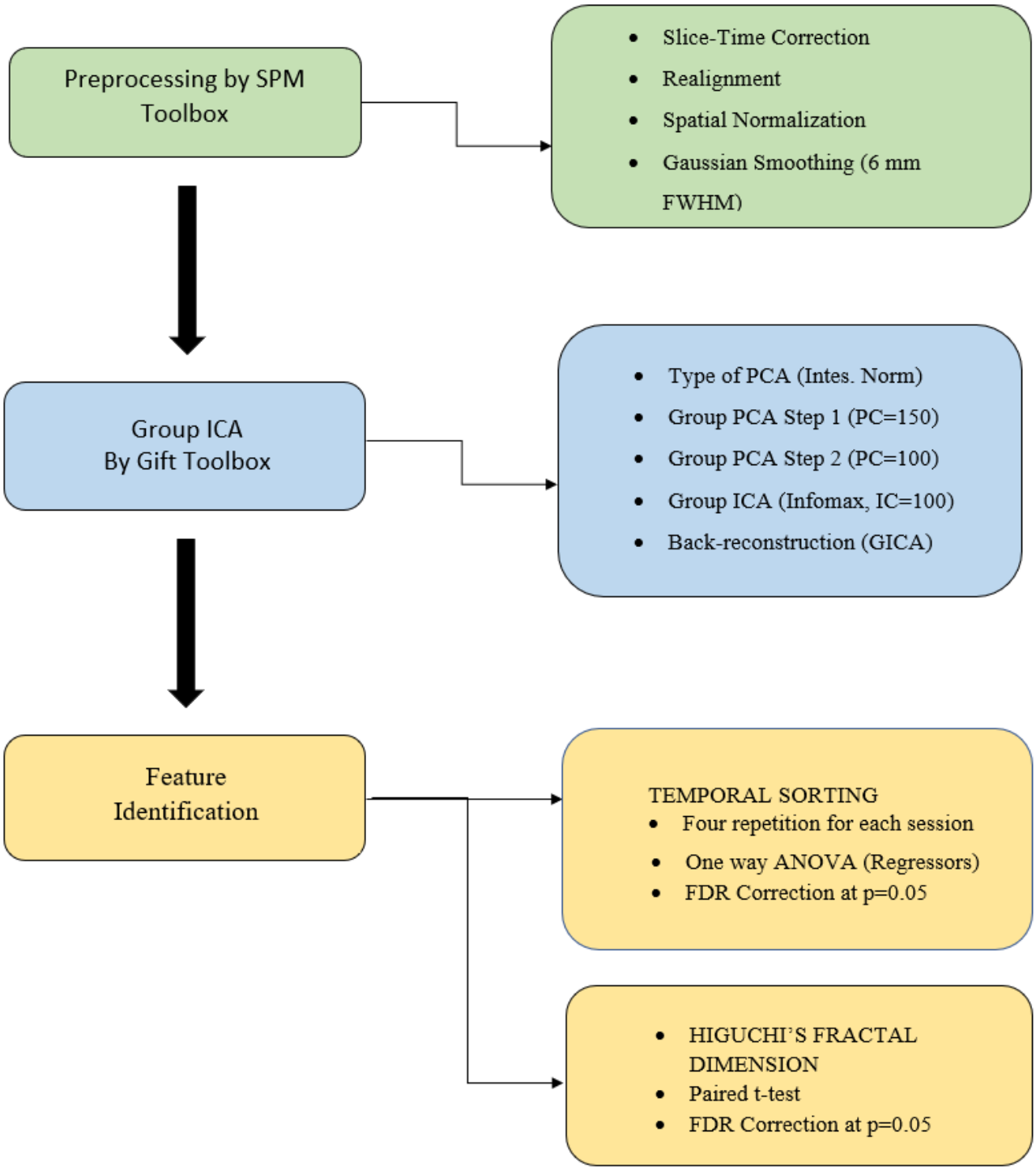

Figure 20. Schematic of the analysis pipeline. Boxes on the left indicate general steps potentially applicable to a variety of data and analysis types; boxes on the right indicate particular choices made for the data and analysis presented here.

4.3.4.3 Task-related networks

In order to compute the degree of task-relatedness of component we regressed the corresponding time-courses against the design matrix, using the temporal multiple linear regression implemented in GIFT. We performed temporal sorting fourth times one for each conditions of interest: Visuomotor (VM), Motor (M), selecting in turn the regressors associated to each condition. Stats on beta weights

option in Utility of GIFT toolbox after temporal sorting was used, it allows one to test the significance of the ICs obtained. The resulting beta weights (β) reflect the degree to which the task events of interest modulated a component. β for each task condition was tested against zero using one-way ANOVA (Regressor). 28 indipendent components (ICs) were selected for the final analysis; only the ICs with a p-value that survived to False Discovery Rate (FDR) correction were considered. ICs were named accordingly to the template (Functional ROIs- https://findlab.stanford.edu/functional_ROIs.html) they were spatially correlated with or based on visual inspection of the corresponding spatial map.

4.3.5 Fractal dimension: Theoretical definition and practical estimation

4.3.5.1 Fractal Analysis

In geometry, fractal objects are peculiar with respect to ordinary shapes because they exhibit self-similarity, i.e. at any scale or level of magnification, they show exact or approximate similarity to a part of themselves (Di Ieva et al. 2014). The complexity or unevenness of fractal patterns can be described by fractal (fractional) dimensions (FDs) that are strictly larger than their topological or geometrical dimension (δ), although being lower than the successive topological dimension (δ + 1). Although FDs seem purely theoretical concepts, they have been employed to model several phenomena in nature (Di Ieva et al. 2014).

In the time domain, FD represents the amplitude of the signal under consideration on a plane as a function of time. As a consequence of this planar geometry, its dimension is limited between 1 and 2, since a simple curve has dimension equal to 1, while a plane has dimension equal to 2. FD will be equal to 2 for time series with high complexity and no memory of the signal (i.e. the overall signal can-not be predicted using an individual portion of the signal), such as white random noise, while it will be equal to 1 for time series with low or no complexity in the signal, such as a ramp line, which is characterized by full memory (i.e. the overall signal using can be predicted using a portion of the signal itself). More-over, it has been demonstrated that higher values of FD correspond to the presence of higher frequencies in the signal's Fourier spectrum and vice versa (Cottone et al. 2017; Klonowski 2007; Zappasodi et al. 2014).

This relationship might not be linear, in fact, has been demonstrated that it was rather quadratic (Marino et al. 2019). There are many methods used to calculate FD, but the widely accepted ones are Katz's and Higuchi's methods, respectively, (Katz 1988) with the latter considered the most accurate to estimate FD (Katz 1988).

4.3.5.2 *Higuchi's fractal dimension*

Higuchi's Fractal Dimension (FD) (Higuchi 1988) is a quantitative measure of signal dynamics. Linear methods commonly used for signal analysis, such as the well-known FFT and wavelet transformation (WT), are good choices if the analyzed signals are stationary. However, neurophysiological processes are generally nonstationary and nonlinear by nature. Knowing that FD is an accurate numerical measure no matter what the properties (stationary, nonstationary, deterministic or stochastic) of the analyzed signal, it is reasonable to accept this advantage over widely used linear methods.

The method for calculating the fractal dimension of a curve in a plane was proposed by Higuchi in 1988 (Higuchi 1988). Higuchi's fractal dimension is a nonlinear measure of waveform complexity in the time domain. Discretized functions or signals could be analyzed as time sequences x(1), x(2),…, x(N), where N is the total number of samples. From the starting time sequence, a new self-similar time series X_k^m was calculated as:

$$X_k^m: x(m), x(m+k), x(m+2k), \ldots, x\left(m + int\left[\frac{N-K}{k}\right]k\right) \tag{4.1}$$

for m = 1, 2,…,k where m is initial time; k is the time interval, k = 1,…, k_{max}; k_{max} is a free parameter, and int(r) is the integer part of the real number r. "The length" of the curve $L_m(k)$ was computed for each of the k time series or curves X_k^m.

$$L_m(k) = \frac{1}{k}\left[\left(\sum_{i=1}^{int[(N-m)/k]} |x(m+ik) - x(m+(i-1)k)|\right)\frac{N-1}{int[\frac{N-m}{k}]k}\right] \tag{4.2}$$

where N is the length of the original time series X and (N−1)/{int[(N − m)/k]k} is a normalization factor. $L_m(k)$ was averaged for all m forming the mean value of the curve length L(k) for each k = 1,…, k_{max} as

$$L(k) = \frac{\sum_{m=1}^{k} L_m(k)}{k}. \tag{4.3}$$

An array of mean values L(k) was obtained and the FD was estimated as the slope of least squares linear best fit from the plot of ln(L(k)) versus ln(1/k):

$$FD = \ln(L(k)) / \ln(1\ k). \tag{4.4}$$

In practice, the original curve or signal can be divided into smaller parts with or without overlapping, called "windows". Then, the method for computing FD values should be applied to each window where N should be seen as the length of the window. So, FD values are calculated for each window, with or without overlap. Individual FD values can be averaged across all windows for the entire curve and the mean FD value can be used as a measure of curve complexity (Porcaro et al. 2020b).

The choice of the free parameter k has a crucial role in FD estimation. For each window we estimated values of FD for k = 7. We have obtained a value of FD for each subject, repeating the procedure for both tasks.

4.3.6 Statistical Analysis

Statistical analysis on beta weights as implemented in GIFT toolbox was performed to identify differences between conditions (M vs. VM). The resulting beta weights (β) reflect the degree to which a component was modulated by the events of interest, i.e. how well did the IC's time course correlate with the condition time-course. To test for FD differences in each ICs between M and VM task, paired t-tests was performed. False discovery rate (FDR) was used to correct for multiple comparisons (Nichols and Holmes 2002).

4.4 Results

4.4.1 GIFT Results

4.4.1.1 Task-related networks

One hundred ICs were identified. Of these, 28 were determined to be task-related after One-Way Anova (Regressor). In the table the results, after One Way ANOVA (Regressor) implementation are reported. P-values and networks for all the components FDR corrected in each condition of interest are present. The components common to the tasks due are highlighted.

VISUOMOTOR			**MOTOR**		
ICs	*p_valueFDR*	*Network*	*ICs*	*p_valueFDR*	*Network*
Visual Network (VN)					
2	0.03	hVN			
3	0.01	pVN			
70	0.007	pVN			
74	**0.001**	**pVN**	**74**	**0.03**	**pVN**
Sensorimotor Network (SMN)					
7	<0.001	iM1			
40	**<0.001**	**cM1**	**40**	**0.001**	**cM1**
92	**0.03**	**SMN**	**92**	**0.03**	**SMN**
Frontal Eye Fields (FEF)					
44	<0.001	FEF			

46	**<0.001**	**FEF**	**46**	**0.02**	**FEF**
Silence Network (SN)					
32	0.003	aSN	64	0.007	aSN
69	<0.001	aSN	89	0.008	aSN
Executive Control Network (ExCN)					
4	**0.001**	**lExCN**	**4**	**0.001**	**lExCN**
54	**0.005**	**rExCN**	**54**	**0.005**	**rExCN**
78	0.02	rExCN			
Default Mode Network (DMN)					
34	0.03	dDMN			
42	**0.02**	**vDMN**	**42**	**0.002**	**vDMN**
68	0.01	dDMN			
83	0.005	dDMN			
Basal Ganglia (BG)					
87	0.02	BG	81	0.009	BG
Cerebellum (CB)					
27	**0.02**	**CB**	**27**	**<0.001**	**CB**
45	**0.04**	**CB**	**45**	**0.007**	**CB**
60	**0.001**	**CB**	**60**	**0.004**	**CB**
			77	0.007	CB
Precuneus					
57	0.005	Prec	49	0.007	Prec

Table 1 ***Task-related components.*** *All the FDR corrected value for each condition are reported.*

In Figure 21 all the fifteen components task-related are shown. These networks included the visual network (IC 2, IC 3, IC 70, IC 74), the Frontal Eye Field (IC 44, IC 46), default mode network (IC 34, IC 42, IC 68, IC 83), silence network (IC 32, IC 64, IC 69, IC 89), executive control network (IC 4, IC 54, IC 78,) sensorimotor network (IC 7, IC 40, IC 92), cerebellum network (IC 27, IC 45, IC 60, IC 77) and basal ganglia (IC 81, IC 87). In the Table 2 we reported the cortical localization of the maximum peak activation for each network.

Figure 21. ***Spatial map (SMs) of the 28 ICs identified as task-related.*** *They are displayed at the three most informative slices (Axial, Sagittal and Coronal views). They are divided into groups based on their anatomical and functional properties and include default mode network, attention network, cerebellum, basal ganglia, sensorimotor network. Each colored circle represents a different condition of interest: red for the Visuomotor condition, blue for the Motor condition.*

	Area	Brodmann Area	Max Value (x, y, z) L/R	MNI (x, y, z)
VISUAL NETWORK				
IC 02	Declive	*	11.4 (-48, -63, -19)/19.9 (48, -57, -19)	(-48, -64, -26)/(48, -58, -26)
	Fusiform Gyrus	19, 37	7.8 (-48, -57, -16)/19.2 (48, -60, -15)	(-48, -58, -22)/(48, -61, -22)
	Tuber	*	5.5 (-45, -52, -23)/13.2 (48, -55, -23)	(-45, -52, -30)/(48, -55, -30)
	Culmen	*	5.2 (-45, -49, -19)/10.8 (45, -49, -19)	(-45, -49, -26)/(45, -49, -26)

	Inferior Temporal Gyrus	20, 37	4.0 (-50, -54, -12)/9.9 (50, -54, -12)	(-51, -55, -18)/(51, -55, -18)
	Sub-Gyral	*	3.1 (-48, -60, -9)/7.3 (48, -63, -9)	(-48, -61, -14)/(48, -64, -14)
	Middle Occipital Gyrus	18, 19, 37	4.1 (-50, -63, -9)/6.6 (42, -68, -8)	(-51, -64, -14)/(42, -70, -14)
IC 03	Lingual Gyrus	17, 18, 19	41.0 (-3, -68, 2)/40.9 (3, -68, 2)	(-3, -70, -2)/(3, -70, -2)
	Cuneus	7, 17, 18, 19, 23, 30	37.6 (-3, -74, 6)/38.1 (3, -74, 6)	(-3, -76, 2)/(3, -76, 2)
	Posterior Cingulate	23, 30, 31	17.9 (-3, -64, 12)/28.5 (6, -67, 13)	(-3, -67, 10)/(6, -70, 10)
	Culmen of Vermis	*	27.8 (0, -65, -2)/25.2 (3, -62, 1)	(0, -67, -6)/(3, -64, -2)
	Culmen	*	24.3 (-6, -65, -2)/26.2 (6, -65, -2)	(-6, -67, -6)/(6, -67, -6)
	Precuneus	23, 31	10.2 (0, -70, 24)/15.6 (3, -67, 20)	(0, -73, 22)/(3, -70, 18)
	Middle Occipital Gyrus	*	7.4 (-27, -62, 5)/8.6 (27, -62, 5)	(-27, -64, 2)/(27, -64, 2)
	Extra-Nuclear	*	6.2 (-24, -62, 9)/8.3 (24, -56, 8)	(-24, -64, 6)/(24, -58, 6)
	Sub-Gyral	37	7.9 (-24, -65, -2)/8.3 (24, -65, -2)	(-24, -67, -6)/(24, -67, -6)
	Declive	*	6.4 (-6, -74, -11)/7.7 (9, -74, -11)	(-6, -76, -18)/(9, -76, -18)
	Fusiform Gyrus	19	4.4 (-21, -65, -8)/7.5 (21, -65, -8)	(-21, -67, -14)/(21, -67, -14)
	Lateral Ventricle	*	5.3 (-27, -65, 9)/7.3 (27, -59, 8)	(-27, -67, 6)/(27, -61, 6)
	Declive of Vermis	*	5.5 (-3, -71, -12)/6.3 (3, -74, -11)	(-3, -73, -18)/(3, -76, -18)
IC 70	Cuneus	17, 18, 19, 23, 30	76.5 (-3, -91, 3)/86.9 (3, -91, 6)	(-3, -94, -2)/(3, -94, 2)
	Lingual Gyrus	17, 18, 19	74.2 (0, -88, 3)/75.0 (3, -91, 0)	(0, -91, -2)/(3, -94, -6)
	Middle Occipital Gyrus	18, 19	32.1 (-12, -91, 14)/48.5 (12, -91, 14)	(-12, -94, 10)/(12, -94, 10)
	Sub-Gyral	*	22.1 (0, -83, -8)/6.1 (24, -82, 2)	(0, -85, -14)/(24, -85, -2)
	Inferior Occipital Gyrus	17	13.0 (-12, -92, -7)/4.1 (18, -89, -7)	(-12, -94, -14)/(18, -91, -14)

	Culmen of Vermis	*	8.6 (-3, -62, 1)/4.3 (3, -62, 1)	(-3, -64, -2)/(3, -64, -2)
	Precuneus	7	7.7 (-3, -68, 49)/3.6 (9, -68, 49)	(-3, -73, 50)/(9, -73, 50)
	Posterior Cingulate	30	6.4 (-3, -59, 8)/7.2 (3, -59, 8)	(-3, -61, 6)/(3, -61, 6)
	Declive	*	4.4 (-6, -83, -18)/5.0 (6, -80, -11)	(-6, -85, -26)/(6, -82, -18)
IC 74	Extra-Nuclear	*	14.9 (-15, -55, 19)/21.2 (15, -55, 19)	(-15, -58, 18)/(15, -58, 18)
	Posterior Cingulate	23, 29, 30, 31	20.5 (-15, -58, 16)/21.0 (12, -56, 16)	(-15, -61, 14)/(12, -58, 14)
	Precuneus	7, 19, 23, 31, 39	18.9 (-9, -64, 20)/20.7 (12, -58, 19)	(-9, -67, 18)/(12, -61, 18)
	Sub-Gyral	*	19.1 (-15, -61, 20)/19.4 (15, -55, 23)	(-15, -64, 18)/(15, -58, 22)
	Cuneus	7, 17, 18, 19, 23, 30	17.7 (-12, -59, 8)/12.3 (9, -59, 8)	(-12, -61, 6)/(9, -61, 6)
	Lingual Gyrus	17, 18, 19	13.6 (-12, -56, 5)/10.9 (15, -53, 5)	(-12, -58, 2)/(15, -55, 2)
	Cingulate Gyrus	31	10.4 (0, -61, 27)/13.2 (12, -55, 27)	(0, -64, 26)/(12, -58, 26)
	Parahippocampal Gyrus	18, 28, 30, 35, 36, 37	10.5 (-12, -50, 4)/10.0 (18, -50, 4)	(-12, -52, 2)/(18, -52, 2)
	Lateral Ventricle	*	8.1 (-27, -56, 12)/10.5 (21, -47, 15)	(-27, -58, 10)/(21, -49, 14)
	Angular Gyrus	39	7.4 (-36, -75, 31)/10.4 (39, -72, 31)	(-36, -79, 30)/(39, -76, 30)
	Middle Temporal Gyrus	19, 39	7.5 (-42, -76, 24)/8.9 (42, -70, 27)	(-42, -79, 22)/(42, -73, 26)
	Superior Occipital Gyrus	19	8.1 (-39, -75, 28)/6.7 (36, -75, 28)	(-39, -79, 26)/(36, -79, 26)
	Superior Temporal Gyrus	22, 39	5.6 (-36, -56, 16)/6.6 (45, -58, 19)	(-36, -58, 14)/(45, -61, 18)
	Culmen	*	4.6 (-9, -56, 1)/5.0 (9, -45, 1)	(-9, -58, -2)/(9, -46, -2)
	Thalamus	*	4.5 (-3, -12, 6)/4.9 (3, -12, 10)	(-3, -13, 6)/(3, -13, 10)
SENSORIMOTOR NETWORK				
IC 07	Precentral Gyrus	4, 6, 13, 43	3.6 (-59, -14, 39)/48.5 (42, -13, 58)	(-60, -16, 42)/(42, -16, 62)

	Postcentral Gyrus	1, 2, 3, 5, 7, 40, 43	4.3 (-56, -10, 43)/39.8 (42, -24, 58)	(-57, -13, 46)/(42, -28, 62)
	Middle Frontal Gyrus	6	3.3 (-33, -1, 61)/33.5 (39, -4, 57)	(-33, -4, 66)/(39, -7, 62)
	Inferior Parietal Lobule	40	3.3 (-45, -33, 55)/24.2 (48, -33, 55)	(-45, -37, 58)/(48, -37, 58)
	Paracentral Lobule	4, 31	3.4 (0, -16, 47)/6.2 (6, -10, 47)	(0, -19, 50)/(6, -13, 50)
	Superior Temporal Gyrus	38	3.3 (-50, 18, -26)/3.2 (56, -7, 6)	(-51, 20, -30)/(57, -7, 6)
IC 40	Precentral Gyrus	4, 6	66.1 (-36, -18, 62)/4.9 (59, -11, 39)	(-36, -22, 66)/(60, -13, 42)
	Postcentral Gyrus	1, 2, 3, 5, 40, 43	58.1 (-45, -16, 54)/6.1 (50, -25, 51)	(-45, -19, 58)/(51, -28, 54)
	Superior Frontal Gyrus	6	38.0 (-30, -9, 65)/3.8 (3, 5, 53)	(-30, -13, 70)/(3, 2, 58)
	Inferior Parietal Lobule	40	29.6 (-45, -33, 55)/3.0 (50, -28, 47)	(-45, -37, 58)/(51, -31, 50)
	Middle Frontal Gyrus	6	24.5 (-33, -4, 61)/5.4 (39, -4, 57)	(-33, -7, 66)/(39, -7, 62)
	Medial Frontal Gyrus	6	10.2 (-3, -1, 50)/6.2 (3, -1, 50)	(-3, -4, 54)/(3, -4, 54)
	Paracentral Lobule	31	9.3 (-3, -10, 47)/3.2 (3, -10, 47)	(-3, -13, 50)/(3, -13, 50)
	Cingulate Gyrus	24, 31	9.2 (-3, -4, 46)/4.3 (3, 1, 46)	(-3, -7, 50)/(3, -1, 50)
IC 92	Inferior Parietal Lobule	2, 40	26.5 (-65, -26, 29)/13.7 (59, -23, 32)	(-66, -28, 30)/(60, -25, 34)
	Postcentral Gyrus	1, 2, 3, 40, 43	26.4 (-62, -22, 36)/20.5 (62, -17, 36)	(-63, -25, 38)/(63, -19, 38)
	Inferior Frontal Gyrus	9, 44, 45	19.6 (-56, 9, 31)/10.7 (59, 15, 23)	(-57, 8, 34)/(60, 14, 26)
	Precentral Gyrus	4, 6, 13, 43, 44	18.1 (-59, -19, 40)/18.1 (59, -16, 40)	(-60, -22, 42)/(60, -19, 42)
	Middle Frontal Gyrus	6, 8, 9	16.5 (-53, 9, 35)/7.7 (56, 9, 35)	(-54, 8, 38)/(57, 8, 38)
	Sub-Gyral	6, 40	11.4 (-36, -37, 37)/9.2 (39, -31, 44)	(-36, -40, 38)/(39, -34, 46)
	Transverse Temporal Gyrus	41, 42	7.8 (-59, -18, 10)/7.4 (62, -12, 13)	(-60, -19, 10)/(63, -13, 14)
	Insula	13, 40	6.7 (-50, -21, 14)/5.3 (50, -18, 17)	(-51, -22, 14)/(51, -19, 18)

	*	*	5.9 (-56, 8, 5)/3.6 (59, 14, 5)	(-57, 8, 6)/(60, 14, 6)
	Middle Temporal Gyrus	37	3.8 (-53, -62, 1)/5.8 (53, -56, -2)	(-54, -64, -2)/(54, -58, -6)
	Inferior Temporal Gyrus	19, 37	4.9 (-53, -68, -2)/5.7 (53, -57, -6)	(-54, -70, -6)/(54, -58, -10)
	Middle Occipital Gyrus	37	3.1 (-53, -68, 5)/4.8 (50, -60, -5)	(-54, -70, 2)/(51, -61, -10)
	Cingulate Gyrus	24	4.7 (0, 4, 31)/3.6 (3, 1, 31)	(0, 2, 34)/(3, -1, 34)
	Extra-Nuclear	*	4.1 (-36, -4, 6)/3.3 (12, -1, -8)	(-36, -4, 6)/(12, -1, -10)
	Superior Frontal Gyrus	6	3.4 (-27, -1, 65)/3.9 (27, -1, 65)	(-27, -4, 70)/(27, -4, 70)
DEFAULT MODE NETWORK				
IC 34	Anterior Cingulate	10, 24, 32, 33	20.8 (0, 35, 19)/20.4 (3, 29, 11)	(0, 35, 22)/(3, 29, 14)
	Cingulate Gyrus	23, 24, 32	20.1 (0, 27, 30)/19.0 (3, 27, 26)	(0, 26, 34)/(3, 26, 30)
	Medial Frontal Gyrus	6, 8, 9, 10, 25, 32	17.1 (0, 41, 18)/19.1 (3, 30, 30)	(0, 41, 22)/(3, 29, 34)
	Extra-Nuclear	*	14.2 (-3, 20, 16)/16.4 (3, 20, 16)	(-3, 20, 18)/(3, 20, 18)
	Sub-Gyral	*	8.6 (-9, 20, 19)/9.5 (9, 31, 8)	(-9, 20, 22)/(9, 32, 10)
	Declive	*	8.7 (-6, -83, -18)/5.1 (6, -80, -14)	(-6, -85, -26)/(6, -82, -22)
	Lateral Ventricle	*	5.8 (-6, 20, 12)/8.4 (6, 20, 12)	(-6, 20, 14)/(6, 20, 14)
	Superior Frontal Gyrus	6, 8, 10	7.8 (-3, 57, -1)/7.5 (3, 57, -1)	(-3, 59, 2)/(3, 59, 2)
	Inferior Frontal Gyrus	46, 47	5.1 (-39, 16, -13)/7.6 (36, 19, -13)	(-39, 17, -14)/(36, 20, -14)
	Caudate	*	3.4 (-12, 8, 9)/4.6 (9, 17, 12)	(-12, 8, 10)/(9, 17, 14)
	Superior Temporal Gyrus	38	4.5 (-45, 13, -9)/4.5 (45, 16, -13)	(-45, 14, -10)/(45, 17, -14)
	Middle Frontal Gyrus	6, 10, 46	4.1 (-39, 43, 11)/4.2 (39, 41, 15)	(-39, 44, 14)/(39, 41, 18)
	Paracentral Lobule	31	4.0 (0, -13, 43)/3.3 (3, -10, 43)	(0, -16, 46)/(3, -13, 46)
	Declive of Vermis	*	3.5 (0, -74, -11)/3.7 (0, -75, -15)	(0, -76, -18)/(0, -76, -22)

	Lingual Gyrus	*	3.5 (-6, -86, -11)/3.0 (3, -83, -8)	(-6, -88, -18)/(3, -85, -14)
	Subcallosal Gyrus	25	3.0 (-3, 13, -12)/3.3 (3, 13, -12)	(-3, 14, -14)/(3, 14, -14)
IC 42	Superior Frontal Gyrus	6, 8, 9, 10	38.4 (-3, 39, 51)/35.6 (9, 45, 47)	(-3, 38, 58)/(9, 44, 54)
	Medial Frontal Gyrus	6, 8, 9, 10	34.4 (-3, 51, 40)/37.1 (6, 56, 36)	(-3, 50, 46)/(6, 56, 42)
	Middle Frontal Gyrus	8, 9, 10, 11	6.7 (-48, 16, 42)/12.3 (48, 21, 41)	(-48, 14, 46)/(48, 20, 46)
	Precentral Gyrus	9	3.6 (-45, 24, 37)/6.6 (45, 24, 37)	(-45, 23, 42)/(45, 23, 42)
	Anterior Cingulate	32	5.0 (-3, 38, 22)/5.8 (3, 38, 22)	(-3, 38, 26)/(3, 38, 26)
	Inferior Frontal Gyrus	9, 47	5.6 (-50, 39, -7)/5.6 (48, 28, -13)	(-51, 41, -6)/(48, 29, -14)
	Cerebellar Tonsil	*	3.3 (-9, -55, -33)/3.2 (6, -55, -33)	(-9, -55, -42)/(6, -55, -42)
IC 68	Precuneus	7, 19, 23, 31, 39	35.2 (0, -52, 30)/31.8 (3, -55, 30)	(0, -55, 30)/(3, -58, 30)
	Cingulate Gyrus	23, 31	33.8 (0, -52, 27)/30.6 (3, -49, 26)	(0, -55, 26)/(3, -52, 26)
	Posterior Cingulate	23, 29, 30, 31	30.3 (0, -49, 23)/26.8 (3, -46, 23)	(0, -52, 22)/(3, -49, 22)
	Cuneus	7	26.0 (0, -64, 31)/18.0 (3, -66, 31)	(0, -67, 30)/(3, -70, 30)
	Sub-Gyral	*	15.8 (-12, -49, 23)/6.4 (15, -46, 23)	(-12, -52, 22)/(15, -49, 22)
	Extra-Nuclear	*	12.0 (-12, -55, 19)/6.2 (3, -41, 15)	(-12, -58, 18)/(3, -43, 14)
	Middle Temporal Gyrus	21, 37, 39	7.4 (-50, -64, 27)/4.6 (50, -58, 23)	(-51, -67, 26)/(51, -61, 22)
	Superior Temporal Gyrus	22, 39	7.2 (-53, -61, 27)/6.2 (53, -55, 27)	(-54, -64, 26)/(54, -58, 26)
	Angular Gyrus	39	7.1 (-45, -69, 35)/5.4 (50, -58, 34)	(-45, -73, 34)/(51, -61, 34)
	Supramarginal Gyrus	40	5.8 (-53, -61, 31)/5.9 (50, -55, 30)	(-54, -64, 30)/(51, -58, 30)
	Postcentral Gyrus	2, 3, 5, 7	3.2 (-48, -30, 55)/5.2 (30, -38, 66)	(-48, -34, 58)/(30, -43, 70)
	Inferior Parietal Lobule	39, 40	5.1 (-45, -66, 38)/4.5 (48, -57, 38)	(-45, -70, 38)/(48, -61, 38)

	Inferior Temporal Gyrus	21, 37	4.2 (-59, -10, -15)/4.7 (50, -65, -2)	(-60, -10, -18)/(51, -67, -6)
	Superior Parietal Lobule	7	3.4 (-36, -69, 46)/4.2 (30, -50, 60)	(-36, -73, 46)/(30, -55, 62)
	Middle Frontal Gyrus	8, 9, 10, 46	3.5 (-48, 21, 38)/3.2 (45, 51, -1)	(-48, 20, 42)/(45, 53, 2)
IC 83	Anterior Cingulate	10, 24, 25, 32	70.1 (-3, 39, -7)/69.2 (3, 39, -7)	(-3, 41, -6)/(3, 41, -6)
	Medial Frontal Gyrus	9, 10	63.3 (-3, 45, -7)/63.4 (3, 45, -7)	(-3, 47, -6)/(3, 47, -6)
	Sub-Gyral	*	38.7 (-12, 48, -7)/38.2 (15, 39, -10)	(-12, 50, -6)/(15, 41, -10)
	Middle Frontal Gyrus	9, 10, 11, 47	34.4 (-18, 42, -11)/33.0 (18, 42, -11)	(-18, 44, -10)/(18, 44, -10)
	Extra-Nuclear	*	27.0 (-3, 28, 0)/26.6 (3, 28, 0)	(-3, 29, 2)/(3, 29, 2)
	Superior Frontal Gyrus	9, 10	21.1 (-9, 51, -1)/26.3 (21, 45, -11)	(-9, 53, 2)/(21, 47, -10)
	Inferior Frontal Gyrus	11, 47	19.6 (-21, 33, -10)/11.1 (24, 31, -10)	(-21, 35, -10)/(24, 32, -10)
	Lateral Ventricle	*	8.8 (-12, 25, 1)/7.6 (9, 22, 1)	(-12, 26, 2)/(9, 23, 2)
	Caudate	*	4.8 (-12, 19, 1)/4.5 (12, 19, -3)	(-12, 20, 2)/(12, 20, -2)
SILENCE NETWORK				
IC 32	Medial Frontal Gyrus	6, 8, 9, 32	20.8 (-3, -4, 54)/22.4 (3, 2, 53)	(-3, -7, 58)/(3, -1, 58)
	Superior Frontal Gyrus	6, 8, 9	18.7 (-3, 8, 53)/20.7 (3, 8, 53)	(-3, 5, 58)/(3, 5, 58)
	Sub-Gyral	6	17.7 (-21, -4, 57)/18.7 (18, -1, 57)	(-21, -7, 62)/(18, -4, 62)
	Middle Frontal Gyrus	6, 8, 9	16.0 (-15, -10, 58)/16.2 (18, -1, 61)	(-15, -13, 62)/(18, -4, 66)
	Cingulate Gyrus	24, 31, 32	12.6 (0, 4, 46)/12.3 (6, 4, 46)	(0, 2, 50)/(6, 2, 50)
	Precentral Gyrus	4, 6	12.1 (-27, -10, 54)/11.4 (33, -7, 54)	(-27, -13, 58)/(33, -10, 58)
	Postcentral Gyrus	2, 3, 4, 5, 40	8.0 (-21, -27, 58)/6.5 (21, -27, 62)	(-21, -31, 62)/(21, -31, 66)
	Superior Parietal Lobule	5, 7	4.2 (-21, -45, 59)/5.1 (21, -39, 59)	(-21, -49, 62)/(21, -43, 62)

	Paracentral Lobule	31	5.1 (-3, -10, 47)/4.9 (3, -10, 47)	(-3, -13, 50)/(3, -13, 50)
	Inferior Frontal Gyrus	9	3.6 (-50, 6, 31)/4.1 (56, 9, 31)	(-51, 5, 34)/(57, 8, 34)
IC 64	Cingulate Gyrus	23, 24, 32	16.8 (-3, 24, 37)/19.1 (3, 24, 37)	(-3, 23, 42)/(3, 23, 42)
	Medial Frontal Gyrus	6, 8, 9, 32	15.5 (-3, 30, 37)/17.2 (3, 30, 37)	(-3, 29, 42)/(3, 29, 42)
	Sub-Gyral	6, 8, 32	16.1 (-24, 13, 42)/15.1 (27, 24, 37)	(-24, 11, 46)/(27, 23, 42)
	Middle Frontal Gyrus	6, 8, 9, 10	15.5 (-24, 19, 41)/15.7 (24, 21, 38)	(-24, 17, 46)/(24, 20, 42)
	Superior Frontal Gyrus	6, 8, 9, 10	14.4 (-21, 16, 45)/12.2 (21, 25, 45)	(-21, 14, 50)/(21, 23, 50)
	Precentral Gyrus	6, 9	6.1 (-39, -2, 42)/10.3 (33, 21, 34)	(-39, -4, 46)/(33, 20, 38)
IC 69	Cingulate Gyrus	24, 31, 32	21.8 (0, -2, 46)/20.7 (3, 1, 42)	(0, -4, 50)/(3, -1, 46)
	Medial Frontal Gyrus	6, 32	18.0 (0, -4, 50)/16.8 (3, -1, 50)	(0, -7, 54)/(3, -4, 54)
	Paracentral Lobule	6, 31	17.9 (-3, -10, 47)/16.6 (3, -10, 47)	(-3, -13, 50)/(3, -13, 50)
	Superior Frontal Gyrus	6, 8, 9, 10	14.4 (-3, 39, 51)/8.8 (9, 39, 51)	(-3, 38, 58)/(9, 38, 58)
	Sub-Gyral	6	12.4 (-21, -7, 46)/11.4 (21, 1, 42)	(-21, -10, 50)/(21, -1, 46)
	Middle Frontal Gyrus	6, 8, 9, 10	11.8 (-24, -4, 46)/11.5 (24, -4, 46)	(-24, -7, 50)/(24, -7, 50)
	Precentral Gyrus	4, 6	10.1 (-24, -10, 50)/7.8 (33, -7, 50)	(-24, -13, 54)/(33, -10, 54)
	Postcentral Gyrus	2, 3, 7	5.9 (-30, -22, 47)/4.2 (18, -50, 67)	(-30, -25, 50)/(18, -55, 70)
	Fusiform Gyrus	18, 19	5.8 (-27, -83, -14)/5.0 (24, -80, -14)	(-27, -85, -22)/(24, -82, -22)
	Declive	*	5.5 (-24, -83, -18)/5.1 (24, -81, -18)	(-24, -85, -26)/(24, -82, -26)
	Lingual Gyrus	18	5.0 (-12, -86, -14)/3.5 (18, -80, -14)	(-12, -88, -22)/(18, -82, -22)
	Subcallosal Gyrus	25	4.4 (-3, 7, -12)/3.1 (3, 7, -12)	(-3, 8, -14)/(3, 8, -14)
	Inferior Frontal Gyrus	9, 44, 45	3.4 (-56, 6, 24)/3.8 (59, 12, 20)	(-57, 5, 26)/(60, 11, 22)

	Superior Parietal Lobule	7	3.5 (-12, -68, 53)/3.0 (24, -59, 60)	(-12, -73, 54)/(24, -64, 62)
	Extra-Nuclear	*	3.1 (-3, -6, 10)/3.4 (3, -15, 14)	(-3, -7, 10)/(3, -16, 14)
IC 89	Superior Temporal Gyrus	21, 22, 38	18.7 (-45, -4, -5)/27.7 (45, 7, -9)	(-45, -4, -6)/(45, 8, -10)
	Extra-Nuclear	13, 47	15.4 (-39, 10, -9)/24.6 (42, 4, -9)	(-39, 11, -10)/(42, 5, -10)
	Inferior Frontal Gyrus	13, 47	17.9 (-42, 13, -9)/22.6 (42, 16, -13)	(-42, 14, -10)/(42, 17, -14)
	Sub-Gyral	21	18.8 (-42, 4, -9)/22.1 (42, -1, -8)	(-42, 5, -10)/(42, -1, -10)
	Insula	13, 22	17.4 (-42, -7, -5)/22.1 (45, 5, -5)	(-42, -7, -6)/(45, 5, -6)
	Lentiform Nucleus	*	8.9 (-27, -7, -5)/14.8 (27, -7, -5)	(-27, -7, -6)/(27, -7, -6)
	Claustrum	*	9.0 (-36, -19, -4)/14.0 (36, -10, -5)	(-36, -19, -6)/(36, -10, -6)
	Parahippocampal Gyrus	28, 34	7.5 (-27, -2, -12)/12.4 (30, -4, -12)	(-27, -1, -14)/(30, -4, -14)
	Middle Temporal Gyrus	21	5.8 (-50, -16, -4)/12.0 (50, 1, -12)	(-51, -16, -6)/(51, 2, -14)
	Subcallosal Gyrus	34	6.5 (-27, 4, -12)/9.7 (21, 4, -12)	(-27, 5, -14)/(21, 5, -14)
	Lateral Ventricle	*	7.2 (-33, -16, -8)/8.2 (33, -16, -8)	(-33, -16, -10)/(33, -16, -10)
	Thalamus	*	5.6 (-3, -15, 3)/6.7 (3, -18, 10)	(-3, -16, 2)/(3, -19, 10)
	Anterior Cingulate	25	4.5 (-3, 19, -6)/5.9 (3, 19, -9)	(-3, 20, -6)/(3, 20, -10)
	Middle Occipital Gyrus	19	3.3 (-39, -82, 10)/3.4 (33, -82, 13)	(-39, -85, 6)/(33, -85, 10)
EXECUTIVE CONTROL NETWORK				
IC 04	Middle Frontal Gyrus	6, 8, 9, 10, 46	35.6 (-50, 21, 34)/13.8 (53, 27, 26)	(-51, 20, 38)/(54, 26, 30)
	Inferior Frontal Gyrus	9, 13, 44, 45, 46, 47	26.0 (-53, 21, 23)/10.1 (56, 26, 19)	(-54, 20, 26)/(57, 26, 22)
	Sub-Gyral	6	21.8 (-45, 20, 19)/10.0 (45, 26, 19)	(-45, 20, 22)/(45, 26, 22)
	Precentral Gyrus	4, 6, 9, 44	21.4 (-45, 21, 34)/8.3 (48, 21, 34)	(-45, 20, 38)/(48, 20, 38)

	*	*	4.4 (0, 36, 33)/4.0 (0, -78, -18)	(0, 35, 38)/(0, -79, -26)
	Medial Frontal Gyrus	6, 8, 9, 32	9.5 (-3, 19, 45)/6.7 (3, 19, 45)	(-3, 17, 50)/(3, 17, 50)
	Superior Frontal Gyrus	6, 8, 9, 10	9.0 (-36, 16, 49)/5.9 (3, 16, 49)	(-36, 14, 54)/(3, 14, 54)
	Cingulate Gyrus	32	8.2 (-3, 19, 41)/5.3 (3, 19, 41)	(-3, 17, 46)/(3, 17, 46)
	Precuneus	7, 19	6.1 (-30, -63, 42)/3.8 (3, -61, 31)	(-30, -67, 42)/(3, -64, 30)
	Cuneus	7	4.7 (0, -64, 31)/3.2 (3, -66, 31)	(0, -67, 30)/(3, -70, 30)
	Anterior Cingulate	32	4.1 (-3, 34, -7)/3.6 (6, 37, -7)	(-3, 35, -6)/(6, 38, -6)
	Postcentral Gyrus	3, 40	3.7 (-53, -10, 47)/3.1 (65, -21, 14)	(-54, -13, 50)/(66, -22, 14)
IC 54	Middle Frontal Gyrus	6, 8, 9, 10, 11, 46, 47	4.7 (-53, 7, 38)/47.8 (42, 51, -11)	(-54, 5, 42)/(42, 53, -10)
	Superior Frontal Gyrus	6, 8, 10	3.6 (-36, 47, 25)/38.1 (33, 60, -8)	(-36, 47, 30)/(33, 62, -6)
	Inferior Frontal Gyrus	9, 45, 46, 47	3.8 (-56, 9, 31)/30.5 (48, 42, -14)	(-57, 8, 34)/(48, 44, -14)
	*	*	4.4 (-21, -31, -24)/22.2 (39, 36, -17)	(-21, -31, -30)/(39, 38, -18)
	Sub-Gyral	20	4.3 (-42, -14, -21)/19.0 (42, 46, 3)	(-42, -13, -26)/(42, 47, 6)
	Medial Frontal Gyrus	8, 10, 25	4.3 (-3, 48, -7)/10.4 (12, 45, -7)	(-3, 50, -6)/(12, 47, -6)
	Middle Temporal Gyrus	21, 22	3.0 (-56, -64, 12)/7.2 (65, -33, -3)	(-57, -67, 10)/(66, -34, -6)
	Precentral Gyrus	6	4.2 (-53, -2, 42)/3.9 (59, 17, 8)	(-54, -4, 46)/(60, 17, 10)
IC 78	Middle Frontal Gyrus	6, 8, 9, 10, 11, 46	5.7 (-50, 29, 22)/34.9 (39, 36, 37)	(-51, 29, 26)/(39, 35, 42)
	Superior Frontal Gyrus	6, 8, 9, 10	5.2 (-3, 39, 51)/33.7 (39, 41, 33)	(-3, 38, 58)/(39, 41, 38)
	Inferior Frontal Gyrus	45, 46, 47	7.5 (-50, 36, -10)/5.2 (45, 43, 7)	(-51, 38, -10)/(45, 44, 10)
	Inferior Parietal Lobule	40	3.5 (-65, -26, 22)/6.6 (45, -48, 52)	(-66, -28, 22)/(45, -52, 54)
	Superior Temporal Gyrus	22, 38	3.0 (-65, -13, 2)/4.8 (30, 18, -26)	(-66, -13, 2)/(30, 20, -30)

BASAL GANGLIA				
IC 81	Subcallosal Gyrus	13, 25, 34, 47	34.3 (-18, 4, -12)/30.7 (18, 7, -12)	(-18, 5, -14)/(18, 8, -14)
	Parahippocampal Gyrus	28, 34	31.6 (-18, 4, -15)/19.2 (21, 4, -15)	(-18, 5, -18)/(21, 5, -18)
	Lentiform Nucleus	*	31.0 (-18, 7, -9)/30.7 (18, 10, -9)	(-18, 8, -10)/(18, 11, -10)
	Extra-Nuclear	13, 47	28.8 (-21, 10, -9)/28.9 (18, 16, -9)	(-21, 11, -10)/(18, 17, -10)
	Inferior Frontal Gyrus	11, 13, 46, 47	26.0 (-21, 7, -15)/24.8 (18, 7, -15)	(-21, 8, -18)/(18, 8, -18)
	Sub-Gyral	*	23.0 (-21, 13, -12)/25.6 (15, 19, -9)	(-21, 14, -14)/(15, 20, -10)
	Medial Frontal Gyrus	25	18.6 (-12, 10, -16)/23.1 (15, 10, -16)	(-12, 11, -18)/(15, 11, -18)
	Uncus	20, 28, 34	21.4 (-18, 4, -19)/11.5 (18, 4, -19)	(-18, 5, -22)/(18, 5, -22)
	Caudate	*	16.5 (-12, 16, -6)/19.2 (12, 19, -6)	(-12, 17, -6)/(12, 20, -6)
	Anterior Cingulate	25	12.9 (-9, 16, -9)/19.0 (9, 13, -9)	(-9, 17, -10)/(9, 14, -10)
	Claustrum	*	14.2 (-27, 13, -6)/12.7 (27, 16, -6)	(-27, 14, -6)/(27, 17, -6)
	Middle Frontal Gyrus	9, 10, 11, 46, 47	7.3 (-24, 30, -17)/10.4 (24, 33, -17)	(-24, 32, -18)/(24, 35, -18)
	Insula	13, 47	7.3 (-27, 19, -6)/5.9 (30, 19, -6)	(-27, 20, -6)/(30, 20, -6)
	Lateral Ventricle	*	6.2 (-27, -10, -11)/3.2 (12, 23, 4)	(-27, -10, -14)/(12, 23, 6)
	Superior Temporal Gyrus	22, 38	6.1 (-30, 10, -19)/3.3 (30, 10, -19)	(-30, 11, -22)/(30, 11, -22)
	Thalamus	*	5.6 (-3, -18, 10)/3.8 (3, -18, 10)	(-3, -19, 10)/(3, -19, 10)
	Superior Frontal Gyrus	10	3.3 (-3, 22, 60)/4.8 (21, 45, -11)	(-3, 20, 66)/(21, 47, -10)
IC 87	Extra-Nuclear	*	42.4 (-3, -6, 13)/44.8 (3, -6, 13)	(-3, -7, 14)/(3, -7, 14)
	Thalamus	*	41.9 (-3, -12, 13)/43.5 (9, -6, 13)	(-3, -13, 14)/(9, -7, 14)
	Caudate	*	30.7 (-9, 0, 13)/39.0 (9, 0, 13)	(-9, -1, 14)/(9, -1, 14)

	Lateral Ventricle	*	27.6 (-3, 0, 13)/32.4 (9, -3, 17)	(-3, -1, 14)/(9, -4, 18)
	Lentiform Nucleus	*	15.2 (-15, 2, 9)/15.6 (18, -1, 9)	(-15, 2, 10)/(18, -1, 10)
	Inferior Frontal Gyrus	47	7.6 (-53, 16, -6)/6.2 (50, 19, -9)	(-54, 17, -6)/(51, 20, -10)
	Superior Temporal Gyrus	22, 38	5.8 (-50, 13, -6)/6.5 (53, 16, -9)	(-51, 14, -6)/(54, 17, -10)
	Posterior Cingulate	23	4.5 (-3, -32, 22)/5.2 (3, -32, 22)	(-3, -34, 22)/(3, -34, 22)
	Sub-Gyral	*	3.2 (-15, 28, -10)/3.8 (39, -11, -21)	(-15, 29, -10)/(39, -10, -26)
	Fourth Ventricle	*	3.0 (-3, -52, -26)/3.6 (0, -49, -26)	(-3, -52, -34)/(0, -49, -34)

FRONTAL EYE FIELD

IC 44	Sub-Gyral	*	5.6 (-33, -43, 37)/12.7 (39, -37, 37)	(-33, -46, 38)/(39, -40, 38)
	Inferior Parietal Lobule	2, 7, 39, 40	4.7 (-36, -52, 38)/12.4 (42, -34, 37)	(-36, -55, 38)/(42, -37, 38)
	Supramarginal Gyrus	40	5.3 (-36, -46, 37)/11.8 (42, -40, 37)	(-36, -49, 38)/(42, -43, 38)
	Postcentral Gyrus	2, 3, 40	3.2 (-42, -28, 36)/9.8 (39, -28, 33)	(-42, -31, 38)/(39, -31, 34)
	Angular Gyrus	39	4.1 (-33, -55, 34)/7.8 (36, -55, 34)	(-33, -58, 34)/(36, -58, 34)
	Precuneus	7, 19, 31, 39	4.5 (-24, -57, 38)/7.0 (24, -54, 41)	(-24, -61, 38)/(24, -58, 42)
	Superior Parietal Lobule	7	3.0 (-27, -57, 45)/6.4 (33, -48, 48)	(-27, -61, 46)/(33, -52, 50)
	Inferior Frontal Gyrus	46, 47	5.8 (-56, 19, -3)/4.2 (53, 16, -6)	(-57, 20, -2)/(54, 17, -6)
	Superior Frontal Gyrus	6, 10	5.5 (-24, 64, 10)/4.2 (18, 14, 64)	(-24, 65, 14)/(18, 11, 70)
	Middle Temporal Gyrus	21, 39	4.0 (-62, -7, -8)/5.4 (36, -58, 27)	(-63, -7, -10)/(36, -61, 26)
	*	*	3.6 (-56, 13, -2)/5.2 (59, 13, -2)	(-57, 14, -2)/(60, 14, -2)
	Superior Temporal Gyrus	21, 22, 39	3.5 (-62, -7, -1)/5.2 (39, -55, 27)	(-63, -7, -2)/(39, -58, 26)
	Medial Frontal Gyrus	10	4.5 (-3, 66, 6)/3.5 (6, 67, 10)	(-3, 68, 10)/(6, 68, 14)

	Anterior Cingulate	24, 33	3.4 (-3, 15, 23)/3.7 (3, 15, 23)	(-3, 14, 26)/(3, 14, 26)
IC 46	Inferior Parietal Lobule	7, 39, 40	9.0 (-45, -42, 56)/38.2 (45, -42, 56)	(-45, -46, 58)/(45, -46, 58)
	Superior Parietal Lobule	7	9.0 (-36, -56, 56)/26.9 (39, -54, 52)	(-36, -61, 58)/(39, -58, 54)
	Postcentral Gyrus	1, 2, 3, 5, 7, 40	5.6 (-39, -39, 59)/24.2 (48, -33, 51)	(-39, -43, 62)/(48, -37, 54)
	Middle Frontal Gyrus	6, 8, 9, 10, 11, 46	5.5 (-42, 52, 7)/13.7 (45, 49, 10)	(-42, 53, 10)/(45, 50, 14)
	Inferior Frontal Gyrus	9, 44, 46	3.4 (-48, 43, 11)/11.0 (48, 43, 11)	(-48, 44, 14)/(48, 44, 14)
	Supramarginal Gyrus	40	3.0 (-59, -43, 37)/9.8 (42, -40, 37)	(-60, -46, 38)/(42, -43, 38)
	Superior Frontal Gyrus	6, 8, 9, 10	5.1 (-39, 52, 14)/8.3 (45, 35, 30)	(-39, 53, 18)/(45, 35, 34)
	Declive	*	3.3 (-9, -80, -14)/4.5 (48, -49, -19)	(-9, -82, -22)/(48, -49, -26)
	Posterior Cingulate	30	3.9 (-18, -65, 9)/3.1 (15, -59, 8)	(-18, -67, 6)/(15, -61, 6)
	Medial Frontal Gyrus	6, 8, 9	3.0 (-3, 38, 29)/3.4 (3, 30, 37)	(-3, 38, 34)/(3, 29, 42)
CEREBELLUM				
IC 27	Fourth Ventricle	*	51.4 (-3, -40, -20)/57.7 (0, -43, -20)	(-3, -40, -26)/(0, -43, -26)
	Culmen	*	49.0 (-3, -46, -20)/45.9 (3, -46, -20)	(-3, -46, -26)/(3, -46, -26)
	Fastigium	*	36.3 (-6, -49, -19)/32.3 (6, -49, -19)	(-6, -49, -26)/(6, -49, -26)
	Nodule	*	27.7 (0, -55, -23)/25.2 (6, -55, -23)	(0, -55, -30)/(6, -55, -30)
	Cerebellar Lingual	*	25.6 (-3, -45, -16)/25.0 (3, -45, -16)	(-3, -46, -22)/(3, -46, -22)
	Declive	*	15.1 (-3, -63, -22)/14.4 (3, -63, -22)	(-3, -64, -30)/(3, -64, -30)
	Pyramis	*	13.8 (0, -63, -25)/9.3 (3, -66, -25)	(0, -64, -34)/(3, -67, -34)
	Uvula	*	11.7 (-6, -61, -29)/11.3 (3, -61, -29)	(-6, -61, -38)/(3, -61, -38)
	Declive of Vermis	*	9.3 (0, -69, -12)/11.6 (0, -66, -22)	(0, -70, -18)/(0, -67, -30)

	Cerebellar Tonsil	*	7.5 (-15, -55, -33)/9.0 (12, -55, -33)	(-15, -55, -42)/(12, -55, -42)
	Inferior Frontal Gyrus	13, 45, 47	3.5 (-24, 18, -19)/7.4 (30, 16, -19)	(-24, 20, -22)/(30, 17, -22)
	Culmen of Vermis	*	6.6 (-3, -65, -8)/6.1 (3, -65, -8)	(-3, -67, -14)/(3, -67, -14)
	Fusiform Gyrus	20, 37	4.9 (-56, -5, -25)/5.7 (48, -60, -15)	(-57, -4, -30)/(48, -61, -22)
	Inferior Temporal Gyrus	20	5.6 (-48, -11, -21)/3.9 (39, -9, -38)	(-48, -10, -26)/(39, -7, -46)
	Superior Temporal Gyrus	38	4.3 (-27, 6, -26)/5.6 (33, 13, -19)	(-27, 8, -30)/(33, 14, -22)
	Extra-Nuclear	*	5.1 (-3, -1, -2)/4.0 (3, -1, -2)	(-3, -1, -2)/(3, -1, -2)
	Middle Temporal Gyrus	21	4.7 (-59, -5, -22)/4.4 (53, 6, -26)	(-60, -4, -26)/(54, 8, -30)
	Anterior Cingulate	25, 32	4.1 (-3, 34, -7)/3.1 (3, 5, -5)	(-3, 35, -6)/(3, 5, -6)
IC 45	Declive	*	19.1 (-24, -69, -15)/28.8 (21, -66, -12)	(-24, -70, -22)/(21, -67, -18)
	Culmen	*	14.2 (-3, -68, -8)/22.9 (9, -68, -8)	(-3, -70, -14)/(9, -70, -14)
	Fusiform Gyrus	19, 37	13.1 (-21, -63, -9)/22.6 (21, -63, -9)	(-21, -64, -14)/(21, -64, -14)
	Lingual Gyrus	18, 19	11.6 (-15, -71, -8)/22.2 (18, -71, -8)	(-15, -73, -14)/(18, -73, -14)
	Declive of Vermis	*	13.6 (0, -69, -12)/16.7 (3, -71, -12)	(0, -70, -18)/(3, -73, -18)
	Sub-Gyral	20	14.1 (-18, -65, -8)/9.6 (30, -62, -5)	(-18, -67, -14)/(30, -64, -10)
	Culmen of Vermis	*	13.5 (0, -65, -8)/11.8 (3, -63, -9)	(0, -67, -14)/(3, -64, -14)
	Parahippocampal Gyrus	19, 36, 37	4.1 (-24, -57, -6)/10.7 (24, -57, -6)	(-24, -58, -10)/(24, -58, -10)
	Tuber	*	6.1 (-42, -55, -23)/6.4 (42, -55, -23)	(-42, -55, -30)/(42, -55, -30)
	Middle Frontal Gyrus	*	3.1 (-30, -1, 61)/3.2 (33, -1, 61)	(-30, -4, 66)/(33, -4, 66)
IC 60	Declive	*	85.8 (-6, -83, -18)/76.3 (6, -81, -18)	(-6, -85, -26)/(6, -82, -26)
	Uvula	*	43.9 (-30, -81, -25)/52.9 (12, -81, -25)	(-30, -82, -34)/(12, -82, -34)

	Pyramis	*	49.3 (-9, -81, -25)/47.5 (3, -78, -25)	(-9, -82, -34)/(3, -79, -34)
	Tuber	*	43.4 (-36, -78, -25)/38.3 (39, -72, -25)	(-36, -79, -34)/(39, -73, -34)
	Declive of Vermis	*	20.5 (0, -71, -12)/40.8 (0, -75, -18)	(0, -73, -18)/(0, -76, -26)
	Lingual Gyrus	18	29.6 (-12, -83, -14)/31.6 (18, -80, -14)	(-12, -85, -22)/(18, -82, -22)
	Tuber of Vermis	*	29.4 (0, -75, -25)/17.4 (3, -72, -25)	(0, -76, -34)/(3, -73, -34)
	Fusiform Gyrus	18, 19, 37	13.5 (-21, -80, -14)/25.3 (24, -80, -14)	(-21, -82, -22)/(24, -82, -22)
	Pyramis of Vermis	*	22.4 (0, -75, -28)/13.5 (3, -72, -28)	(0, -76, -38)/(3, -73, -38)
	Culmen	*	5.8 (-27, -63, -25)/9.0 (6, -68, -8)	(-27, -64, -34)/(6, -70, -14)
	Inferior Temporal Gyrus	20	3.8 (-45, -8, -28)/8.8 (39, -9, -38)	(-45, -7, -34)/(39, -7, -46)
	Cerebellar Tonsil	*	8.5 (-36, -64, -32)/5.5 (3, -49, -36)	(-36, -64, -42)/(3, -49, -46)
	Culmen of Vermis	*	8.1 (0, -65, -5)/8.4 (3, -65, -8)	(0, -67, -10)/(3, -67, -14)
	Postcentral Gyrus	7	6.7 (-9, -47, 67)/5.8 (6, -47, 67)	(-9, -52, 70)/(6, -52, 70)
	Fourth Ventricle	*	3.5 (-3, -40, -20)/5.3 (0, -43, -20)	(-3, -40, -26)/(0, -43, -26)
	Sub-Gyral	*	3.1 (-50, -11, -18)/4.0 (36, -13, -14)	(-51, -10, -22)/(36, -13, -18)
	Extra-Nuclear	*	3.6 (-3, -24, 7)/3.8 (3, -21, 10)	(-3, -25, 6)/(3, -22, 10)
	Thalamus	*	3.8 (-3, -18, 6)/3.5 (3, -18, 6)	(-3, -19, 6)/(3, -19, 6)
	Middle Frontal Gyrus	6, 10	3.0 (-27, 11, 60)/3.5 (27, 63, 6)	(-27, 8, 66)/(27, 65, 10)
	Superior Frontal Gyrus	10	3.3 (-12, 66, 6)/3.4 (27, 63, 2)	(-12, 68, 10)/(27, 65, 6)
	Medial Frontal Gyrus	*	3.3 (-3, -27, 66)/3.0 (3, 53, 36)	(-3, -31, 70)/(3, 53, 42)
IC 77	Nodule	*	103.1 (-3, -46, -30)/87.5 (3, -46, -30)	(-3, -46, -38)/(3, -46, -38)
	Cerebellar Tonsil	*	78.2 (0, -49, -36)/48.0 (6, -49, -33)	(0, -49, -46)/(6, -49, -42)
	Fourth Ventricle	*	21.4 (-3, -52, -26)/77.8 (0, -49, -33)	(-3, -52, -34)/(0, -49, -42)

	Uvula	*	16.5 (-6, -61, -32)/13.3 (6, -61, -32)	(-6, -61, -42)/(6, -61, -42)
	Declive	*	6.9 (-45, -69, -22)/3.2 (33, -78, -18)	(-45, -70, -30)/(33, -79, -26)
	Superior Temporal Gyrus	38	5.8 (-36, 10, -22)/6.5 (39, 13, -19)	(-36, 11, -26)/(39, 14, -22)
	Pyramis	*	6.1 (-18, -61, -29)/6.0 (18, -61, -29)	(-18, -61, -38)/(18, -61, -38)
	Culmen	*	5.7 (-6, -40, -20)/3.2 (6, -40, -20)	(-6, -40, -26)/(6, -40, -26)
	Pyramis of Vermis	*	5.2 (-3, -75, -28)/4.5 (3, -69, -28)	(-3, -76, -38)/(3, -70, -38)
	Inferior Temporal Gyrus	20	4.4 (-45, -8, -28)/5.1 (39, -9, -38)	(-45, -7, -34)/(39, -7, -46)
	Thalamus	*	4.7 (-3, -15, 3)/5.0 (3, -9, 6)	(-3, -16, 2)/(3, -10, 6)
	Fusiform Gyrus	20	3.6 (-48, -8, -25)/3.1 (27, -57, -9)	(-48, -7, -30)/(27, -58, -14)
PRECUNEUS				
IC 49	Cingulate Gyrus	23, 24, 31	31.7 (0, -26, 29)/29.7 (3, -29, 29)	(0, -28, 30)/(3, -31, 30)
	Extra-Nuclear	*	28.0 (-3, -23, 25)/23.5 (6, -20, 25)	(-3, -25, 26)/(6, -22, 26)
	Posterior Cingulate	23	27.7 (-3, -29, 25)/28.1 (3, -29, 25)	(-3, -31, 26)/(3, -31, 26)
	Lateral Ventricle	*	17.7 (-3, -17, 21)/16.9 (6, -20, 21)	(-3, -19, 22)/(6, -22, 22)
	Paracentral Lobule	5, 6, 31	13.2 (0, -31, 44)/11.7 (3, -28, 44)	(0, -34, 46)/(3, -31, 46)
	Precuneus	7, 31	11.3 (-3, -34, 44)/11.3 (3, -34, 44)	(-3, -37, 46)/(3, -37, 46)
	Sub-Gyral	*	10.1 (-18, -32, 29)/10.5 (21, -29, 29)	(-18, -34, 30)/(21, -31, 30)
	Caudate	*	6.3 (-18, -20, 25)/9.9 (18, -20, 25)	(-18, -22, 26)/(18, -22, 26)
	Thalamus	*	6.7 (-6, -18, 17)/7.5 (6, -18, 17)	(-6, -19, 18)/(6, -19, 18)
	Superior Frontal Gyrus	8, 10	7.0 (-24, 64, 10)/3.5 (21, 48, 40)	(-24, 65, 14)/(21, 47, 46)
	Middle Temporal Gyrus	21, 22	5.0 (-62, -51, -6)/4.7 (62, -45, -3)	(-63, -52, -10)/(63, -46, -6)
	Superior Temporal Gyrus	22	3.0 (-62, -50, 12)/3.6 (62, -38, 7)	(-63, -52, 10)/(63, -40, 6)

IC 57	Extra-Nuclear	*	30.5 (-3, -35, 18)/30.8 (3, -35, 18)	(-3, -37, 18)/(3, -37, 18)
	Posterior Cingulate	23, 29, 30, 31	28.2 (-3, -41, 19)/28.0 (3, -32, 22)	(-3, -43, 18)/(3, -34, 22)
	Cingulate Gyrus	23, 24, 31	20.8 (0, -32, 26)/18.3 (3, -35, 26)	(0, -34, 26)/(3, -37, 26)
	Lateral Ventricle	*	15.7 (-6, -23, 21)/13.7 (12, -32, 15)	(-6, -25, 22)/(12, -34, 14)
	Thalamus	*	10.8 (-12, -26, 14)/11.9 (12, -26, 14)	(-12, -28, 14)/(12, -28, 14)
	Sub-Gyral	*	8.7 (-6, -44, 11)/8.3 (6, -44, 11)	(-6, -46, 10)/(6, -46, 10)
	Caudate	*	7.9 (-15, -23, 18)/6.1 (18, -26, 18)	(-15, -25, 18)/(18, -28, 18)
	Precuneus	7, 31	3.9 (0, -46, 30)/4.9 (12, -66, 35)	(0, -49, 30)/(12, -70, 34)
	Middle Frontal Gyrus	8, 9, 10	4.7 (-39, 27, 41)/3.1 (36, 37, 11)	(-39, 26, 46)/(36, 38, 14)
	Insula	13	4.5 (-30, -26, 14)/4.7 (36, -35, 18)	(-30, -28, 14)/(36, -37, 18)
	Anterior Cingulate	24, 25, 33	4.5 (-3, 2, -5)/4.3 (3, 31, -3)	(-3, 2, -6)/(3, 32, -2)
	Superior Temporal Gyrus	13, 21, 22, 41	3.6 (-65, -15, 3)/4.3 (36, -32, 15)	(-66, -16, 2)/(36, -34, 14)
	Inferior Frontal Gyrus	44, 47	4.2 (-53, 31, -10)/3.6 (42, 17, 12)	(-54, 32, -10)/(42, 17, 14)
	Precentral Gyrus	9	3.3 (-36, 24, 37)/3.0 (42, 17, 8)	(-36, 23, 42)/(42, 17, 10)
	Cuneus	7, 17	3.0 (-6, -91, 3)/3.2 (9, -66, 31)	(-6, -94, -2)/(9, -70, 30)

Table 3 Attribute manipulation: Motor vs. Visuomotor. Cortical localizations of the for contrast-related independents components (ICs): for each IC, we presented the anatomical location, corresponding Brodmann areas (BAs) and max value with its Montreal Institute Montreal Neurological Institute (MNI) coordinates(obtained using the Talairach utility provided in GIFT toolbox on group-ICA components maps).

4.4.1.2 One Way ANOVA between Motor and Visuomotor

Three ICs, behaved differently during M vs. VN task (Fig. 22 and Table 3). IC40 within the contralateral Sensorimotor network (cSMN), including Precentral and Postcentral Gyrus with maximum activation, positively correlated with M task but negatively with the VM task. The positive correlation with the motor task was stronger than VM correlation. (IC35, cSMN, T= -1.301, p= 0.019). IC74 within the primary Visual Network (pVN) showed a strong positive correlation with the

Visuomotor than Motor task (IC74, pVN, T= 2.377, p= 0.027). Finally, IC75 again within pVN showed the opposite effect (IC38, SN, T= −2.729, p=0.01) with stronger effects during Motor task.

	Area	Brodmann Area	Max Value (x, y, z)	MNI (x, y, z)
Sensorimotor Network (SMN)				
IC 40	Precentral Gyrus	4, 6	66.1/4.9	(-36, -22, 66)/(60, -13, 42)
	Postcentral Gyrus	1, 2, 3, 5, 40, 43	58.1/6.1	(-45, -19, 58)/(51, -28, 54)
	Superior Frontal Gyrus	6	38.0/3.8	(-30, -13, 70)/(3, 2, 58)
	Inferior Parietal Lobule	40	29.6/3.0	(-45, -37, 58)/(51, -31, 50)
	Middle Frontal Gyrus	6	24.5/5.4	(-33, -7, 66)/(39, -7, 62)
	Medial Frontal Gyrus	6	10.2/6.2	(-3, -4, 54)/(3, -4, 54)
	Paracentral Lobule	31	9.3/3.2	(-3, -13, 50)/(3, -13, 50)
	Cingulate Gyrus	24, 31	9.2/4.3	(-3, -7, 50)/(3, -1, 50)
Visual Network (VN)				
IC 74	Extra-Nuclear	*	14.9/21.2	(-15, -58, 18)/(15, -58, 18)
	Posterior Cingulate	23, 29, 30, 31	20.5/21.0	(-15, -61, 14)/(12, -58, 14)
	Precuneus	7, 19, 23, 31, 39	18.9/20.7	(-9, -67, 18)/(12, -61, 18)
	Sub-Gyral	*	19.1/19.4	(-15, -64, 18)/(15, -58, 22)
	Cuneus	7, 17, 18, 19, 23, 30	17.7/12.3	(-12, -61, 6)/(9, -61, 6)
	Lingual Gyrus	17, 18, 19	13.6/10.9	(-12, -58, 2)/(15, -55, 2)
	Cingulate Gyrus	31	10.4/13.2	(0, -64, 26)/(12, -58, 26)
	Parahippocampal Gyrus	18, 28, 30, 35, 36, 37	10.5/10.0	(-12, -52, 2)/(18, -52, 2)
	Lateral Ventricle	*	8.1/10.5	(-27, -58, 10)/(21, -49, 14)
	Angular Gyrus	39	7.4/10.4	(-36, -79, 30)/(39, -76, 30)
	Middle Temporal Gyrus	19, 39	7.5/8.9	(-42, -79, 22)/(42, -73, 26)
	Superior Occipital Gyrus	19	8.1/6.7	(-39, -79, 26)/(36, -79, 26)
	Superior Temporal Gyrus	22, 39	5.6/6.6	(-36, -58, 14)/(45, -61, 18)
	Culmen	*	4.6/5.0	(-9, -58, -2)/(9, -46, -2)
	Thalamus	*	4.5/4.9	(-3, -13, 6)/(3, -13, 10)
	Paracentral Lobule	5	3.8/3.3	(0, -43, 50)/(3, -40, 50)
	Middle Frontal Gyrus	6	3.7/3.4	(-33, -4, 66)/(36, 59, 10)
IC 75	Culmen	*	35.8/32.4	(-9, -58, -2)/(9, -52, -2)
	Lingual Gyrus	17, 18, 19	35.1/35.8	(-12, -55, -2)/(12, -49, -2)
	Parahippocampal Gyrus	19, 27, 28, 30, 35, 36, 37	26.0/32.2	(-12, -43, -2)/(15, -52, 2)
	Culmen of Vermis	*	26.5/24.9	(0, -61, -2)/(6, -61, -2)
	Posterior Cingulate	23, 29, 30, 31	19.8/24.2	(-3, -58, 6)/(15, -55, 6)
	Sub-Gyral	*	23.3/20.1	(-15, -43, -6)/(21, -46, -2)
	Extra-Nuclear	*	8.6/19.7	(-24, -61, 6)/(21, -55, 6)
	Cuneus	7, 17, 18, 19, 23, 30	18.3/16.6	(-12, -61, 6)/(3, -64, 6)
	Fusiform Gyrus	19, 20, 37	10.7/5.5	(-21, -55, -14)/(24, -52, -14)
	Lateral Ventricle	*	4.6/9.9	(-27, -58, 6)/(27, -55, 6)
	Middle Occipital Gyrus	18	8.7/6.5	(-27, -64, 2)/(27, -64, 2)
	Cerebellar Lingual	*	6.8/7.0	(-3, -43, -14)/(6, -46, -14)
	Precuneus	19, 23, 31	5.4/4.1	(-6, -82, 38)/(12, -61, 18)
	Declive	*	5.1/4.6	(-18, -61, -18)/(18, -55, -18)

Table 3 Attribute manipulation: Motor vs. Visuomotor. Cortical localizations of the for contrast-related independents components (ICs): for each IC, we presented the anatomical location, corresponding Brodmann areas (BAs) and max value with its Montreal Institute Montreal Neurological Institute (MNI) coordinates(obtained using the Talairach utility provided in GIFT toolbox on group-ICA components maps).

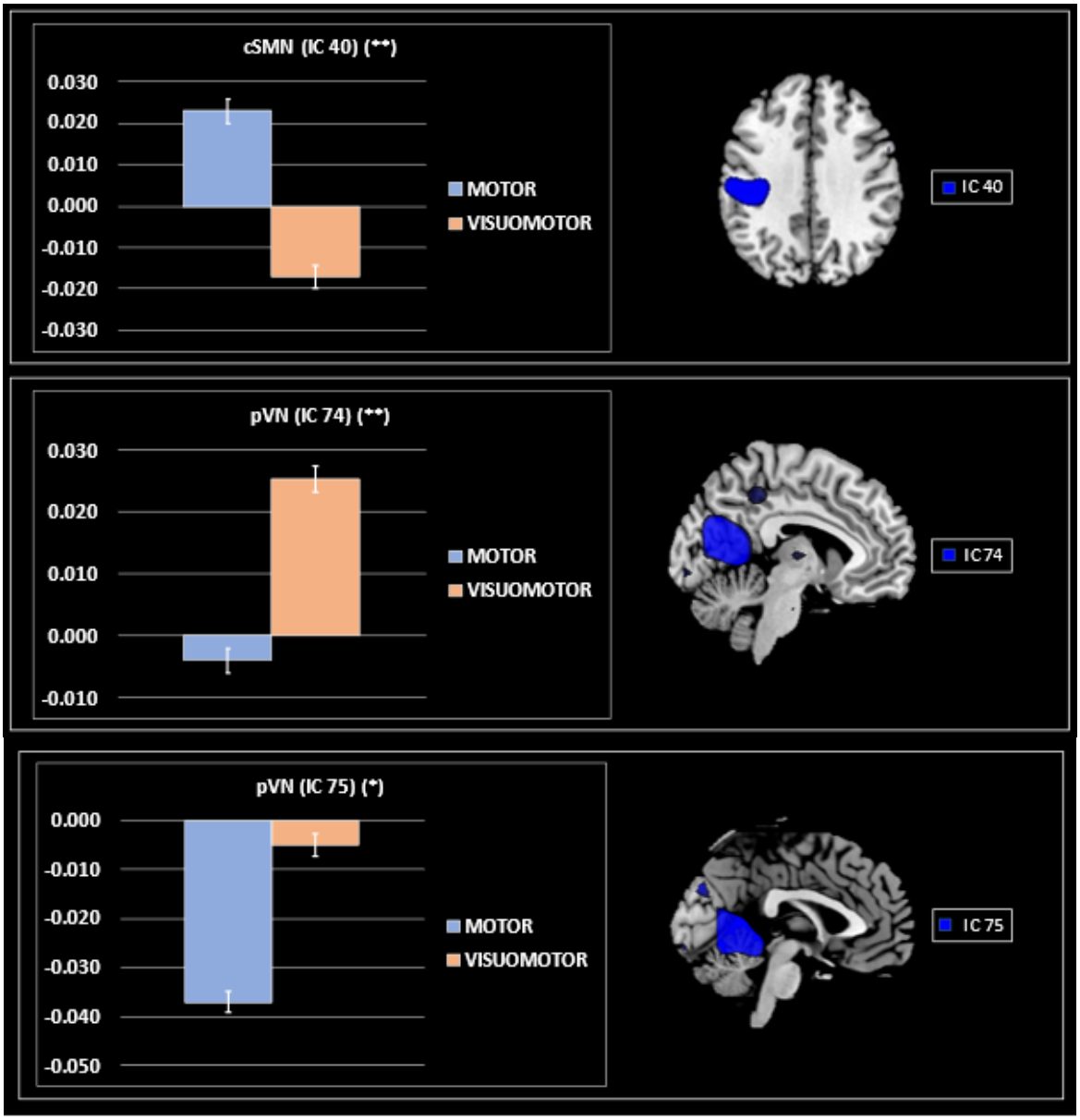

*Figure 22. The plots represented effects size for the ICNs (y-axis beta efect size in arbitrary units). Labels: MOTOR: NoFeedback Task; VISUOMOTOR: Feedback task. ** indicates p<0.01 FDR corrected; * indicate p<0.05 FDR corrected*

4.4.1.3 Higuchi's Fractal Dimension

The hemodynamic FD analysis highlighted sixteen ICs with statistical differences between M and VM tasks significance. Figure 23 shows the ICs, grouped by the network showing the grand average and standard error for the FD and the relative spatial map. At the univariate level, the FD values of the VM task differ from those of the M task. Higher FD values were observed for the VM than for the M task.

Significant components (Figure 23) include the VN, both pVN and hVN, the SMN, both bilateral M1 and iM1, the FEF, the ExCN and Cb. The components belonging to the same networks were averaged between them and compared in the two task.

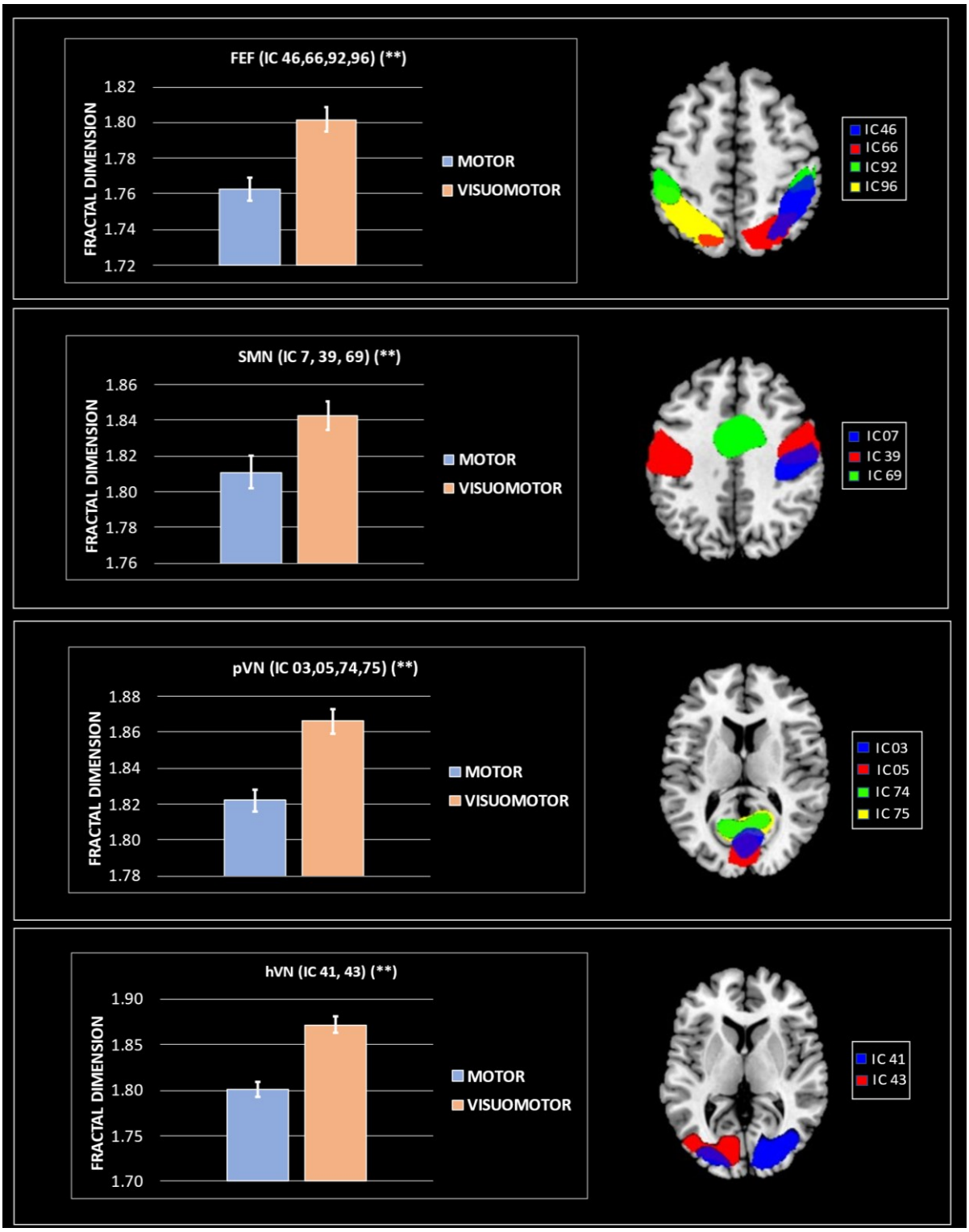

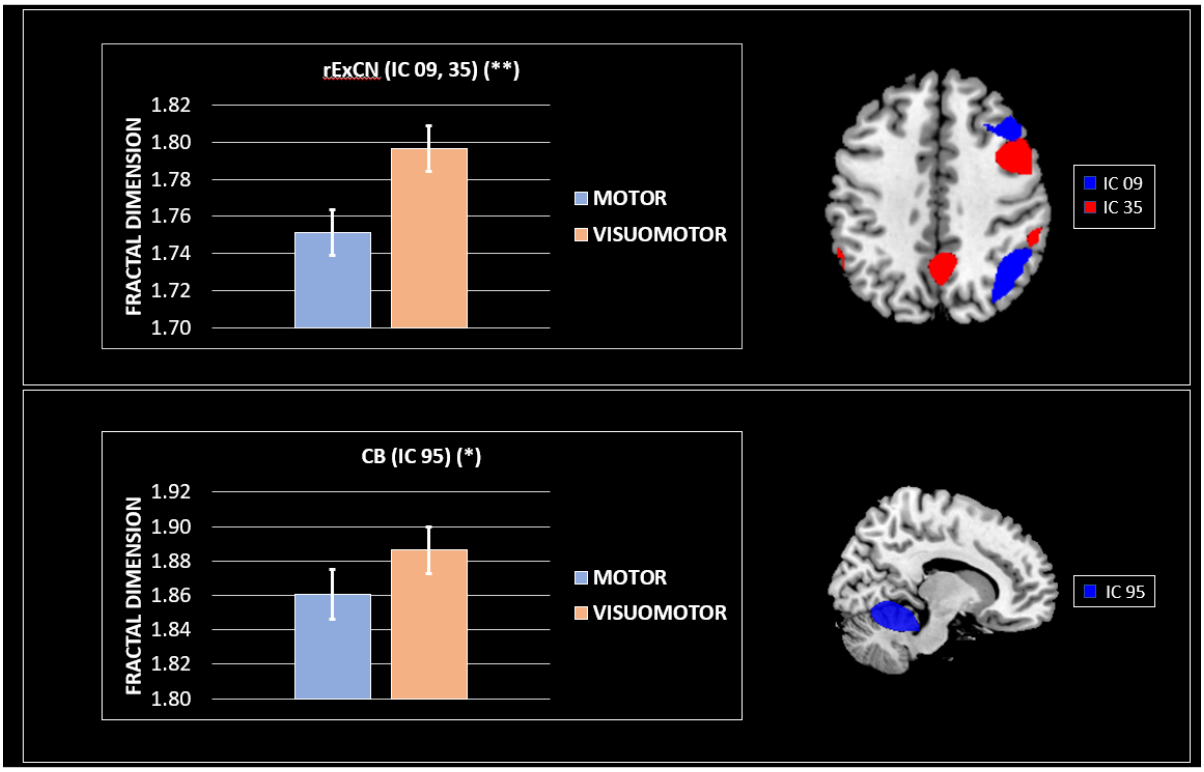

*Figure 23. Hemodynamic activity characterization by Fractal Dimension. For each panel: to the right grand average and standard error for the FD values (k = 7) are shown for both groups M (light blue) and VM (light orange) and to the left spatial maps of the IC obtained by GIFT toolbox. * indicates p<0.05;** indicate p<0.01*

4.5 CONCLUSION

Understanding the mechanisms underlying fine motor control is crucial, not only for basic scientific knowledge but also to optimize rehabilitation strategies following brain injury or in relation to aging. (Heuninckx, Wenderoth, and Swinnen 2010; Prodoehl et al. 2013; López-Larraz et al. 2018)

In this thesis, we analyzed fMRI data recorded during an isometric contraction using a multivariate data-driven approach focusing on intrinsic connectivity between voxels through group ICA. The choice to use the activity-based spatial ICA data-driven approach is due to the fact that the data-driven approach a more advantageous approach over conventional mass-univariate analysis of signal amplitude change, as it is not based on hypotheses regarding the trend of time, the temporal characteristics and the shape of the hemodynamic response function.

This analysis enabled us to identify ipsilateral primary motor cortex (iM1) as the area associated with accurately maintaining a stable and precise isometric contraction under conditions of visual feedback, while the other nodes of the visuomotor network were necessary for performance of the task in both conditions (with and without visual feedback). The contralateral primary motor cortex (CM1) is active during both tasks: its activation describes the arrangement whereby the motor cortex of each cerebral hemisphere is primarily responsible for controlling the movements of the contralateral (opposite) side of the body. More generally, the activity of the motor components is however different between two tasks, as the complexity of the same is greater in the presence of a visual feedback. As expected, the visual netwrok shows its greatest activation during the visuomotor task, especially the pVN. The visual network nodes are involved in visual processing and activated during visual stimuli. In support of this, the fractal dimension shows greater complexity for both pVN and hVN during the execution of the visuomotor task. The interaction of the visual field with the FEF allows the processing of the signal, by means of the control that the FEF has on the ocular movements. The components of the FEF are more correlated with the visuomotor task and the study using the FD shows a greater complexity of this network in the presence of visual feedback. This analysis highlights that, during the visuomotor task, the involvement of FEF appears to be essential for fine motor control of movement in maintaining visual force from feedback, as is the case for the previously described iM1.

The study of complexity has allowed us to identify the ExCN, the SN and the DMN, as areas more associated with the support of the visuomotor task than the motor one. The ExCN interacts with the Vn receiving visual stimuli and, integrating them with the sensorimotor inputs, gives a response relating to the activity to be performed. Its activity is moderated by the SN, Its activity is moderated by the SN, it initiates the dynamic transition between CEN and DMN to mediate between attention

to endogenous and exogenous events. The considered the moderator of the mind, which constantly monitors the outside world and carefully decides how other brain networks react to new information or stimuli. The basal ganglia and cerebellum also differ between the two tasks, showing more complex activity in the VM: the BG supports visuomotor integration when performing a visuomotor task with precision force with the right hand (Papadelis et al. . 2016), while the Cb is able to transfer visual information into correct signals to alter the motor output in progress (Tzvi, Loens, and Donchin 2022).

In general, we can say that the brain networks, although active in both, all show greater complexity in the presence of visual feedback, for the processing of the visual stimulus and for the maintenance of the required level of force.

REFERENCE

"(PDF) An Extension of The Herault-Jutten Network to Signals Including Delays for Blind Separation." n.d. Accessed October 12, 2022. https://www.researchgate.net/publication/2323200_An_Extension_of_The_Herault-Jutten_Network_to_Signals_Including_Delays_for_Blind_Separation.

Beaty, Roger E., Mathias Benedek, Scott Barry Kaufman, and Paul J. Silvia. 2015. "Default and Executive Network Coupling Supports Creative Idea Production." *Scientific Reports* 5 (June). https://doi.org/10.1038/SREP10964.

Bedini, Marco, and Daniel Baldauf. 2021. "Structure, Function and Connectivity Fingerprints of the Frontal Eye Field versus the Inferior Frontal Junction: A Comprehensive Comparison." *The European Journal of Neuroscience* 54 (4): 5462–5506. https://doi.org/10.1111/ejn.15393.

Bell, Anthony J., and Terrence J. Sejnowski. 1995. "An Information-Maximization Approach to Blind Separation and Blind Deconvolution." *Neural Computation* 7 (6): 1129–59. https://doi.org/10.1162/neco.1995.7.6.1129.

Bilevicius, Elena, Tiffany A. Kolesar, Stephen D. Smith, Paul D. Trapnell, and Jennifer Kornelsen. 2018. "Trait Emotional Empathy and Resting State Functional Connectivity in Default Mode, Salience, and Central Executive Networks." *Brain Sciences 2018, Vol. 8, Page 128* 8 (7): 128. https://doi.org/10.3390/BRAINSCI8070128.

Bordier, Cécile, Michel Dojat, and Pierre Lafaye de Micheaux. 2011. "Temporal and Spatial Independent Component Analysis for FMRI Data Sets Embedded in the AnalyzeFMRI R Package." *Journal of Statistical Software* 44 (9): 1–24. https://doi.org/10.18637/JSS.V044.I09.

Calhoun, V. D., T. Adali, G. D. Pearlson, and J. J. Pekar. 2001. "A Method for Making Group Inferences from Functional MRI Data Using Independent Component Analysis." *Human Brain Mapping* 14 (3): 140–51. https://doi.org/10.1002/HBM.1048.

Chang, Edward F., Caroline A. Niziolek, Robert T. Knight, Srikantan S. Nagarajan, and John F. Houde. 2013. "Human Cortical Sensorimotor Network Underlying Feedback Control of Vocal Pitch." *Proceedings of the National Academy of Sciences of the United States of America* 110 (7): 2653–58. https://doi.org/10.1073/PNAS.1216827110/SUPPL_FILE/PNAS.201216827SI.PDF.

Corbetta, Maurizio, and Gordon L. Shulman. 2002. "Control of Goal-Directed and Stimulus-Driven Attention in the Brain." *Nature Reviews Neuroscience 2002 3:3* 3 (3): 201–15. https://doi.org/10.1038/nrn755.

Cottone, Carlo, Camillo Porcaro, Andrea Cancelli, Elzbieta Olejarczyk, Carlo Salustri, and Franca Tecchio. 2017. "Neuronal Electrical Ongoing Activity as a Signature of Cortical Areas." *Brain Structure and Function* 222 (5): 2115–26. https://doi.org/10.1007/s00429-016-1328-4.

Daniels, Judith K., Alexander C. McFarlane, Robyn L. Bluhm, Kathryn A. Moores, C. Richard Clark, Marnie E. Shaw, Peter C. Williamson, Maria Densmore, and Ruth A. Lanius. 2010. "Switching between Executive and Default Mode Networks in Posttraumatic Stress Disorder: Alterations in Functional Connectivity." *Journal of Psychiatry & Neuroscience : JPN* 35 (4): 258–66. https://doi.org/10.1503/JPN.090175.

Eickhoff, S. B., and V. I. Müller. 2015. "Functional Connectivity." *Brain Mapping: An Encyclopedic Reference* 2 (February): 187–201. https://doi.org/10.1016/B978-0-12-397025-1.00212-8.

Ekhtiari, Hamed, Padideh Nasseri, Fatemeh Yavari, Azarkhsh Mokri, and John Monterosso. 2016. "Neuroscience of Drug Craving for Addiction Medicine: From Circuits to Therapies." *Progress*

in Brain Research 223 (January): 115–41. https://doi.org/10.1016/BS.PBR.2015.10.002.

Engel, Andreas K., Pascal Fries, and Wolf Singer. 2001. "Dynamic Predictions: Oscillations and Synchrony in Top–down Processing." *Nature Reviews Neuroscience 2001 2:10* 2 (10): 704–16. https://doi.org/10.1038/35094565.

Friston, Karl J. 2011. "Functional and Effective Connectivity: A Review." *Brain Connectivity* 1 (1): 13–36. https://doi.org/10.1089/BRAIN.2011.0008.

Gillebert, Céline R., and Dante Mantini. 2013. "Functional Connectivity in the Normal and Injured Brain." *The Neuroscientist : A Review Journal Bringing Neurobiology, Neurology and Psychiatry* 19 (5): 509–22. https://doi.org/10.1177/1073858412463168.

Giussani, Carlo, Frank Emmanuel Roux, Jeffrey Ojemann, Erik Pietro Sganzerla, David Pirillo, and Costanza Papagno. 2010. "Is Preoperative Functional Magnetic Resonance Imaging Reliable for Language Areas Mapping in Brain Tumor Surgery? Review of Language Functional Magnetic Resonance Imaging and Direct Cortical Stimulation Correlation Studies." *Neurosurgery* 66 (1): 113–20. https://doi.org/10.1227/01.NEU.0000360392.15450.C9.

Glover, Gary H. n.d. "Overview of Functional Magnetic Resonance Imaging." https://doi.org/10.1016/j.nec.2010.11.001.

Goel, Vinod, Christian Buchel, Chris Frith, and Raymond J. Dolan. 2000. "Dissociation of Mechanisms Underlying Syllogistic Reasoning." *NeuroImage* 12 (5): 504–14. https://doi.org/10.1006/nimg.2000.0636.

Goodale, Melvyn A., and A. David Milner. 1992. "Separate Visual Pathways for Perception and Action." *Trends in Neurosciences* 15 (1): 20–25. https://doi.org/10.1016/0166-2236(92)90344-8.

Gordon, J., and C. Ghez. 1987. "Trajectory Control in Targeted Force Impulses - III. Compensatory Adjustments for Initial Errors." *Experimental Brain Research* 67 (2): 253–69. https://doi.org/10.1007/BF00248547.

Greicius, Michael D., Ben Krasnow, Allan L. Reiss, and Vinod Menon. 2003. "Functional Connectivity in the Resting Brain: A Network Analysis of the Default Mode Hypothesis." *Proceedings of the National Academy of Sciences of the United States of America* 100 (1): 253–58. https://doi.org/10.1073/PNAS.0135058100/SUPPL_FILE/5058TABLE7.HTML.

Hendee, W R, and C J Morgan. 1984. "Magnetic Resonance Imaging. Part I--Physical Principles." *The Western Journal of Medicine* 141 (4): 491–500. http://www.ncbi.nlm.nih.gov/pubmed/6506686.

Heuninckx, S., N. Wenderoth, and S.P. Swinnen. 2010. "Age-Related Reduction in the Differential Pathways Involved in Internal and External Movement Generation." *Neurobiology of Aging* 31 (2): 301–14. https://doi.org/10.1016/j.neurobiolaging.2008.03.021.

Higuchi, T. 1988. "Approach to an Irregular Time Series on the Basis of the Fractal Theory." *Physica D: Nonlinear Phenomena* 31 (2): 277–83. https://doi.org/10.1016/0167-2789(88)90081-4.

Hikosaka, Okihide, Yoriko Takikawa, and Reiko Kawagoe. 2000. "Role of the Basal Ganglia in the Control of Purposive Saccadic Eye Movements." *Physiological Reviews* 80 (3): 953–78. https://doi.org/10.1152/PHYSREV.2000.80.3.953.

Horovitz, Silvina, Anees Abrol, Brian Caffo, Jaroslaw Harezlak, Maria A Kudela, Mario Dzemidzic, Brandon G Oberlin, Zikai Lin, Joaquín Goñi, and David A Kareken. 2019. "Semiparametric Estimation of Task-Based Dynamic Functional Connectivity on the Population Level." *Frontiers*

in Neuroscience | Www.Frontiersin.Org 1: 583. https://doi.org/10.3389/fnins.2019.00583.

Hyvärinen, Aapo, Aapo Hyvärinen, and Erkki Oja. 1999. "Independent Component Analysis: A Tutorial." http://130.203.136.95/viewdoc/summary?doi=10.1.1.374.8694.

Ieva, A. Di, F. Grizzi, H. Jelinek, A. J. Pellionisz, and G. A. Losa. 2014. "Fractals in the Neurosciences, Part I: General Principles and Basic Neurosciences." *The Neuroscientist* 20 (4): 403–17. https://doi.org/10.1177/1073858413513927.

Katz, Michael J. 1988. "Fractals and the Analysis of Waveforms." *Computers in Biology and Medicine* 18 (3): 145–56. https://doi.org/10.1016/0010-4825(88)90041-8.

Klonowski, Wlodzimierz. 2007. "From Conformons to Human Brains: An Informal Overview of Nonlinear Dynamics and Its Applications in Biomedicine." *Nonlinear Biomedical Physics* 1 (1): 5. https://doi.org/10.1186/1753-4631-1-5.

Lam, Tania, and Keir G. Pearson. 2002. "The Role of Proprioceptive Feedback in the Regulation and Adaptation of Locomotor Activity." *Advances in Experimental Medicine and Biology* 508: 343–55. https://doi.org/10.1007/978-1-4615-0713-0_40.

Lanciego, J. L., N. Luquin, and J. A. Obeso. 2012. "Functional Neuroanatomy of the Basal Ganglia." *Cold Spring Harbor Perspectives in Medicine* 2 (12): a009621–a009621. https://doi.org/10.1101/cshperspect.a009621.

Lee, Megan H., Carl D. Hacker, Abraham Z. Snyder, Maurizio Corbetta, Dongyang Zhang, Eric C. Leuthardt, and Joshua S. Shimony. 2012. "Clustering of Resting State Networks." *PLOS ONE* 7 (7): e40370. https://doi.org/10.1371/JOURNAL.PONE.0040370.

Li, Kaiming, Lei Guo, Jingxin Nie, Gang Li, and Tianming Liu. 2008. "Review of Methods for Functional Brain Connectivity Detection Using FMRI." https://doi.org/10.1016/j.compmedimag.2008.10.011.

López-Larraz, Eduardo, Jaime Ibáñez, Fernando Trincado-Alonso, Esther Monge-Pereira, José Luis Pons, and Luis Montesano. 2018. "Comparing Recalibration Strategies for Electroencephalography-Based Decoders of Movement Intention in Neurological Patients with Motor Disability." *International Journal of Neural Systems* 28 (07): 1750060. https://doi.org/10.1142/S0129065717500605.

Louro, Ricardo O. 2013. "Introduction to Biomolecular NMR and Metals." *Practical Approaches to Biological Inorganic Chemistry*, January, 77–107. https://doi.org/10.1016/B978-0-444-56351-4.00004-X.

Mansi, Silvia Angela, Medaglia Maria Teresa, Stefano Seri, Paolo Tonin, Pia Rotshtein, and Camillo Porcaro. 2022. "Frontal Intrinsic Connectivity Networks Support Contradiction Identification During Inductive and Deductive Reasoning." *Cognitive Computation* 14 (2): 677–92. https://doi.org/10.1007/s12559-021-09982-y.

Marino, Marco, Quanying Liu, Jessica Samogin, Franca Tecchio, Carlo Cottone, Dante Mantini, and Camillo Porcaro. 2019. "Neuronal Dynamics Enable the Functional Differentiation of Resting State Networks in the Human Brain." *Human Brain Mapping* 40 (5): 1445–57. https://doi.org/10.1002/hbm.24458.

Martuzzi, Roberto, Ramachandran Ramani, Maolin Qiu, Xilin Shen, Xenophon Papademetris, and R. Todd Constable. 2011. "A Whole-Brain Voxel Based Measure of Intrinsic Connectivity Contrast Reveals Local Changes in Tissue Connectivity with Anesthetic without a Priori Assumptions on Thresholds or Regions of Interest." *NeuroImage* 58 (4): 1044–50.

https://doi.org/10.1016/J.NEUROIMAGE.2011.06.075.

Mayhew, Stephen D., Camillo Porcaro, Franca Tecchio, and Andrew P. Bagshaw. 2017. “FMRI Characterisation of Widespread Brain Networks Relevant for Behavioural Variability in Fine Hand Motor Control with and without Visual Feedback.” *NeuroImage* 148 (January): 330–42. https://doi.org/10.1016/j.neuroimage.2017.01.017.

Montirosso, Rosario, Milena Peverelli, Elisa Frigerio, Monica Crespi, and Renato Borgatti. 2010. “The Development of Dynamic Facial Expression Recognition at Different Intensities in 4- to 18-Year-Olds.” *Social Development* 19 (1): 71–92. https://doi.org/10.1111/j.1467-9507.2008.00527.x.

Mustari, Michael J., Seiji Ono, and Vallabh E. Das. 2009. “Signal Processing and Distribution in Cortical-Brainstem Pathways for Smooth Pursuit Eye Movements.” *Annals of the New York Academy of Sciences* 1164 (1): 147–54. https://doi.org/10.1111/j.1749-6632.2009.03859.x.

Neuper, Christa, Michael Wörtz, and Gert Pfurtscheller. 2006. “ERD/ERS Patterns Reflecting Sensorimotor Activation and Deactivation.” *Progress in Brain Research* 159: 211–22. https://doi.org/10.1016/S0079-6123(06)59014-4.

Nichols, Thomas E., and Andrew P. Holmes. 2002. “Nonparametric Permutation Tests for Functional Neuroimaging: A Primer with Examples.” *Human Brain Mapping* 15 (1): 1–25. https://doi.org/10.1002/hbm.1058.

Niendam, Tara A., Angela R. Laird, Kimberly L. Ray, Y. Monica Dean, David C. Glahn, and Cameron S. Carter. 2012. “Meta-Analytic Evidence for a Superordinate Cognitive Control Network Subserving Diverse Executive Functions.” *Cognitive, Affective, & Behavioral Neuroscience 2012 12:2* 12 (2): 241–68. https://doi.org/10.3758/S13415-011-0083-5.

Nieto-Castanon, Alfonso. 2021. “CONN Functional Connectivity Toolbox (RRID:SCR_009550), Version 21.” https://doi.org/10.56441/HILBERTPRESS.2161.7292.

Nomura, Tatsuya, Masaki Eguchi, Hiroaki Niwamoto, Humio Kokubo, and Masayuki Miyamoto. 1996. “Extension of the Herault-Jutten Network to Signals Including Delays for Blind Separation.” *Neural Networks for Signal Processing - Proceedings of the IEEE Workshop*, 443–52. https://doi.org/10.1109/NNSP.1996.548374.

Ogawa, S., R. S. Menon, D. W. Tank, S. G. Kim, H. Merkle, J. M. Ellermann, and K. Ugurbil. 1993. “Functional Brain Mapping by Blood Oxygenation Level-Dependent Contrast Magnetic Resonance Imaging. A Comparison of Signal Characteristics with a Biophysical Model.” *Biophysical Journal* 64 (3): 803. https://doi.org/10.1016/S0006-3495(93)81441-3.

Ogawa, S., D. W. Tank, R. Menon, J. M. Ellermann, S. G. Kim, H. Merkle, and K. Ugurbil. 1992. “Intrinsic Signal Changes Accompanying Sensory Stimulation: Functional Brain Mapping with Magnetic Resonance Imaging.” *Proceedings of the National Academy of Sciences of the United States of America* 89 (13): 5951. https://doi.org/10.1073/PNAS.89.13.5951.

Ogawa, Seiji, T. M. Lee, and Bertrand Barrere. 1993. “The Sensitivity of Magnetic Resonance Image Signals of a Rat Brain to Changes in the Cerebral Venous Blood Oxygenation.” *Magnetic Resonance in Medicine* 29 (2): 205–10. https://doi.org/10.1002/MRM.1910290208.

Ogawa, Seiji, Tso-Ming -M Lee, Asha S. Nayak, and Paul Glynn. 1990. “Oxygenation-Sensitive Contrast in Magnetic Resonance Image of Rodent Brain at High Magnetic Fields.” *Magnetic Resonance in Medicine* 14 (1): 68–78. https://doi.org/10.1002/MRM.1910140108.

Ortiz-Rosario, Alexis, and Hojjat Adeli. 2013. “Brain-Computer Interface Technologies: From Signal

to Action.” *Reviews in the Neurosciences* 24 (5): 537–52. https://doi.org/10.1515/REVNEURO-2013-0032.

Pfurtscheller, G., and F. H. Lopes Da Silva. 1999. “Event-Related EEG/MEG Synchronization and Desynchronization: Basic Principles.” *Clinical Neurophysiology* 110 (11): 1842–57. https://doi.org/10.1016/S1388-2457(99)00141-8.

“Physical Principles of Magnetic Resonance Imaging - PubMed.” n.d. Accessed October 12, 2022. https://pubmed.ncbi.nlm.nih.gov/2663291/.

Porcaro, Camillo, Stephen D. Mayhew, and Andrew P. Bagshaw. 2021. “Role of the Ipsilateral Primary Motor Cortex in the Visuo-Motor Network during Fine Contractions and Accurate Performance.” *International Journal of Neural Systems* 31 (6): 1–17. https://doi.org/10.1142/S0129065721500118.

Porcaro, Camillo, Stephen D. Mayhew, Marco Marino, Dante Mantini, and Andrew P. Bagshaw. 2020a. “Characterisation of Haemodynamic Activity in Resting State Networks by Fractal Analysis.” *International Journal of Neural Systems* 30 (12): 1–15. https://doi.org/10.1142/S0129065720500616.

———. 2020b. “Characterisation of Haemodynamic Activity in Resting State Networks by Fractal Analysis.” *International Journal of Neural Systems* 30 (12): 2050061. https://doi.org/10.1142/S0129065720500616.

Prodoehl, Janey, Peggy J. Planetta, Ajay S. Kurani, Cynthia L. Comella, Daniel M. Corcos, and David E. Vaillancourt. 2013. “Differences in Brain Activation Between Tremor- and Nontremor-Dominant Parkinson Disease.” *JAMA Neurology* 70 (1): 100. https://doi.org/10.1001/jamaneurol.2013.582.

Raichle, Marcus E., Ann Mary MacLeod, Abraham Z. Snyder, William J. Powers, Debra A. Gusnard, and Gordon L. Shulman. 2001. “A Default Mode of Brain Function.” *Proceedings of the National Academy of Sciences of the United States of America* 98 (2): 676–82. https://doi.org/10.1073/PNAS.98.2.676/ASSET/0D756665-76C2-42A2-ACA7-01DE9C6DEDA4/ASSETS/GRAPHIC/PQ0115125005.JPEG.

Sale, Alessandro, Elena Putignano, Laura Cancedda, Silvia Landi, Francesca Cirulli, Nicoletta Berardi, and Lamberto Maffei. 2004. “Enriched Environment and Acceleration of Visual System Development.” *Neuropharmacology* 47 (5): 649–60. https://doi.org/10.1016/j.neuropharm.2004.07.008.

Seeger, L L. 1989. “Physical Principles of Magnetic Resonance Imaging.” *Clinical Orthopaedics and Related Research*, no. 244 (July): 7–16. http://www.ncbi.nlm.nih.gov/pubmed/2663291.

Silva, Afonso C., Sang-Pil Lee, Costantino Iadecola, and Seong-Gi Kim. 2000. “Early Temporal Characteristics of Cerebral Blood Flow and Deoxyhemoglobin Changes during Somatosensory Stimulation.” *Journal of Cerebral Blood Flow & Metabolism* 20 (1): 201–6. https://doi.org/10.1097/00004647-200001000-00025.

Stevens, Michael C., Kent A. Kiehl, Godfrey D. Pearlson, and Vince D. Calhoun. 2007. “Functional Neural Networks Underlying Response Inhibition in Adolescents and Adults.” *Behavioural Brain Research* 181 (1): 12–22. https://doi.org/10.1016/J.BBR.2007.03.023.

STOODLEY, C, and J SCHMAHMANN. 2009. “Functional Topography in the Human Cerebellum: A Meta-Analysis of Neuroimaging Studies.” *NeuroImage* 44 (2): 489–501. https://doi.org/10.1016/j.neuroimage.2008.08.039.

Tzvi, Elinor, Sebastian Loens, and Opher Donchin. 2022. “Mini-Review: The Role of the Cerebellum in Visuomotor Adaptation.” *The Cerebellum* 21 (2): 306–13. https://doi.org/10.1007/s12311-021-01281-4.

Verstynen, Timothy, Jörn Diedrichsen, Neil Albert, Paul Aparicio, and Richard B. Ivry. 2005a. “Ipsilateral Motor Cortex Activity during Unimanual Hand Movements Relates to Task Complexity.” *Journal of Neurophysiology* 93 (3): 1209–22. https://doi.org/10.1152/JN.00720.2004/ASSET/IMAGES/LARGE/Z9K0030544610007.JPEG.

———. 2005b. “Ipsilateral Motor Cortex Activity during Unimanual Hand Movements Relates to Task Complexity.” *Journal of Neurophysiology* 93 (3): 1209–22. https://doi.org/10.1152/JN.00720.2004.

Verstynen, Timothy, and Richard B. Ivry. 2011. “Network Dynamics Mediating Ipsilateral Motor Cortex Activity during Unimanual Actions.” *Journal of Cognitive Neuroscience* 23 (9): 2468–80. https://doi.org/10.1162/JOCN.2011.21612.

Vessel, Edward A., Ayse Ilkay Isik, Amy M. Belfi, Jonathan L. Stahl, and G. Gabrielle Starr. 2019. “The Default-Mode Network Represents Aesthetic Appeal That Generalizes across Visual Domains.” *Proceedings of the National Academy of Sciences of the United States of America* 116 (38): 19155–64. https://doi.org/10.1073/PNAS.1902650116/SUPPL_FILE/PNAS.1902650116.SAPP.PDF.

Vogel, Alecia C., Fran M. Miezin, Steven E. Petersen, and Bradley L. Schlaggar. 2012. “The Putative Visual Word Form Area Is Functionally Connected to the Dorsal Attention Network.” *Cerebral Cortex (New York, N.Y. : 1991)* 22 (3): 537–49. https://doi.org/10.1093/CERCOR/BHR100.

Wijk, B. C.M. Van, A. Daffertshofer, N. Roach, and P. Praamstra. 2009. “A Role of Beta Oscillatory Synchrony in Biasing Response Competition?” *Cerebral Cortex* 19 (6): 1294–1302. https://doi.org/10.1093/cercor/bhn174.

Wirth, Miranka, Kay Jann, Thomas Dierks, Andrea Federspiel, Roland Wiest, and Helge Horn. 2011. “Semantic Memory Involvement in the Default Mode Network: A Functional Neuroimaging Study Using Independent Component Analysis.” *NeuroImage* 54 (4): 3057–66. https://doi.org/10.1016/J.NEUROIMAGE.2010.10.039.

Zappasodi, Filippo, Elzbieta Olejarczyk, Laura Marzetti, Giovanni Assenza, Vittorio Pizzella, and Franca Tecchio. 2014. “Fractal Dimension of EEG Activity Senses Neuronal Impairment in Acute Stroke.” Edited by Helmut Ahammer. *PLoS ONE* 9 (6): e100199. https://doi.org/10.1371/journal.pone.0100199.